NERC Scientific Support and Facilities
Ion Microprobe Facility

University of Edinburgh
NERC Ion Microprobe Facility

2020 Annual Science Report

Ion Microprobe Facility
School of Geosciences
Kings Buildings
James Hutton Road
Edinburgh
EH9 3FE

https://www.ed.ac.uk/geosciences/about/facilities/all/ionprobe

Contents

Groundtruthing the $\delta^{11}B$ pH proxy in coral aragonite

N. Allison

School of Earth and Environmental Sciences, University of St. Andrews, St Andrews, KY16 9AL, UK

Introduction

Corals build their skeletons from a seawater based calcification fluid isolated in an extracellular space between the base of the coral organism and the underlying skeleton. Recent studies indicate that corals increase the pH of this fluid (pH_{CF}) above that of seawater [1], that pH_{CF} is positively correlated with seawater pH [2] and that coral calcification rates are strongly influenced with the concentrations of different dissolved inorganic carbon species in the fluid [3]. Coral skeletal boron geochemistry offers opportunities to probe the pH and DIC chemistry of this fluid [4] and to explore past seawater pH, controls on coral reef development and the future response to ocean acidification. In this project we aim to compare estimates of coral calcification fluid pH and $[CO_3^{2-}]$ from boron geochemistry of coral skeletons with direct estimates based on observations of a fluorescent pH sensitive dye and measurements using microsensors from comparable sections of a coral skeleton. Our ultimate aim is to confirm if skeletal $\delta^{11}B$ and B/Ca indicate calcification fluid pH and DIC accurately or if other unresolved factors act to fractionate skeletal $\delta^{11}B$ and B/Ca.

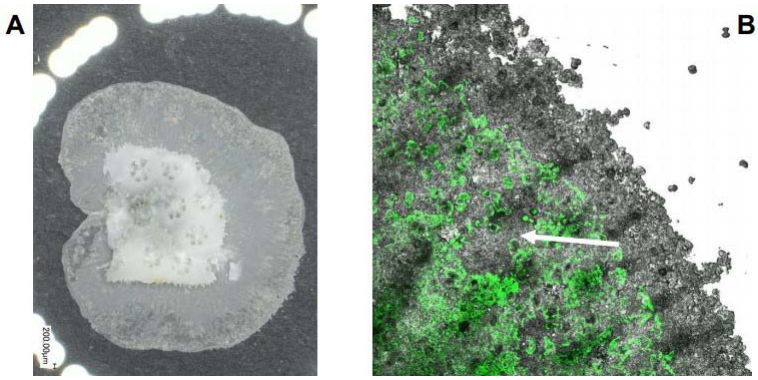

Fig. 1. a) A Stylophora sp. coral grown on a glass coverslip (image width is 9 mm), b) superimposed confocal microscope images of calcein stain and aragonite crystals at the coral growth edge (image width is 1 mm). Images are superimposed but were collected simultaneously. The calcein stain indicates the growth front of the coral at the start of the experiment. The white arrow indicates what would have been a gap in the growing skeleton. This would have held a pocket of calcification fluid which was analysed by LIX and SNARF. The fluid was eventually used to build the skeleton to fill the gap.

Results

The samples for this study were prepared by growing chips of corals on glass coverslips (Figure 1a). Calcification site pH was estimated from inverted confocal microscope observations of the fluorescent pH sensitive dye SNARF in pockets of calcification fluid at the edge of the growing coral [1] and both pH and $[CO_3^{2-}]$ were estimated by inserting liquid ion exchange (LIX) microsensors into similar fluid pockets [5]. SNARF and LIX measurements were made over a 3-4 day period in both the light and dark. At the start of this period the corals were stained with calcein, a dye incorporated into the growing aragonite that can be used to record the positions of the growing crystals. At the end of the experimental period corals were sacrificed, cleaned with sodium hypochlorite and imaged to record the position of the calcein stain. We can resolve gaps in the calcein stain which indicate the positions of fluid pockets used for SNARF and LIX measurements (Figure 1b). After cleaning, coral chips were embedded in epoxy resin and polished to remove the glass coverslip whilst leaving the underlying coral aragonite for SIMS analysis (Figure 2). To identify the positions of what would have been calcification fluid pockets during the culturing experiment with the aragonite in the SIMS section, we correlated the positions of pockets identified in the calcein maps (imaged before polishing) with the micrographs produced after polishing using unique features in the coral section such as voids in the section and dark spots (see Figure 1b) which are likely to be centres of calcification i.e. the start points of aragonite deposition.

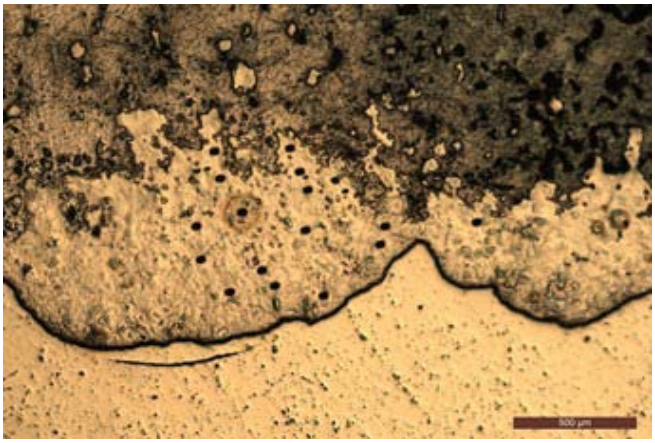

Fig. 2. Reflected light micrograph of area analysed by SIMS. The bottom third of the image shows the glass slide overlying the sample. The top third shows epoxy resin. In between these 2 areas is the polished carbonate. Black dots are SIMS pits. The scale bar is 500 µm.

SIMS analysis were made using the Cameca 7f. A chip of a Desmophyllum spp. cold water coral skeleton which exhibits limited heterogeneity in B/Ca and $\delta^{11}B$ (1σ is 3% and 1.2 ‰ respectively) was measured daily to confirm that instrument drift was insignificant between days. We analysed the $\delta^{11}B$ and B/Ca of the aragonite crystals deposited at the sites used for SNARF dye and microsensor measurements, making multiple analyses (n= 5-23) within each site. Figure 3 shows mean $^{10}B/^{11}B$ of 3 areas from one cultured coral sample. The maximum variation between sites is 0.0006 ($^{10}B/11B$) equivalent to a change in seawater pH of ~0.15 pH units. This indicates that pH variations in the calcification fluid are relatively small over the study period. SNARF dye and LIX microsensors both record pH with a precision (1σ) of 0.1 units. To calculate the absolute $\delta^{11}B$ of the sample (and accurately reconstruct calcification fluid pH) we conducted multiple SIMS analyses on a cultured coral skeleton (which exhibits low $\delta^{11}B$ heterogeneity) in the same SIMS session. We have drilled this coral and will now determine $\delta^{11}B$ by bulk methods.

We will compare the calcifying fluid pH and [CO_3^{2-}] estimates from SIMS analysis with the direct measurements by dye and microsensors. We will confirm if skeletal $\delta^{11}B$ and B/Ca indicate calcification fluid pH and DIC accurately or if other unresolved factors act to fractionate skeletal $\delta^{11}B$ and influence DIC. Dye and microsensor measurements can only be made at the growth edges of living coral specimens in the laboratory. In contrast skeletal boron geochemistry offers opportunities to resolve calcification fluid pH and [CO_3^{2-}] in both modern and fossil field coral specimens and to understand how coral biomineralisation has reacted to past and present climate change. Confirmation that skeletal $\delta^{11}B$ and B/Ca reflect calcification fluid chemistry accurately will facilitate the development of this proxy.

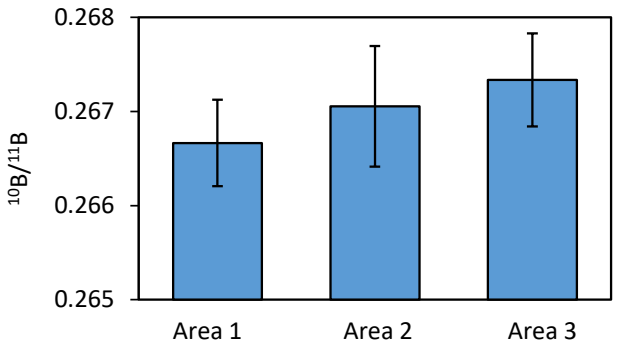

Fig. 3. Mean $^{10}B/^{11}B$ of multiple SIMS analyses in the locations of 3 areas identified to be fluid pockets.

References

[1] A.A. Venn et al. (2011) PLoS ONE 6, e20013. [2] S. Reynaud et al. (2004) Coral Reefs 23, 539-547. [3] N. Allison et al. (2018) Chemical Geology 497, 162-169. [4] N. Allison et al. (2014) Nature Communications 5, 5741 doi: 10.1038/ncomms6741. [5] S.V. Sevilgen et al. (2019) Science Advances, DOI: 10.1126/sciadv.aau7447

Oxygen isotopic distribution along the otolith growth axis by secondary ion mass spectrometry: Application for studying life history of yellowfin tuna (*Thunnus albacares*)

I. Artetxe-Arrate[1], I. Fraile[1] & H. Murua[2]

[1]AZTI, Marine Research, Basque Research and Technology Alliance (BRTA), Pasaia, Gipuzkoa, 20110, Spain
[2]International Seafood Sustainability Foundation, Washington, DC 20005, USA.

Oxygen isotope ($\delta^{18}O$) composition in otolith aragonite is influenced by both the isotopic composition and the temperature of the ambient water, being inversely related with the latter [1,2]. Otolith $\delta^{18}O$ from fish otoliths is commonly used to discriminate marine stocks, but, variations in otolith $\delta^{18}O$ can also be used as a natural geolocator for deciphering lifetime movements of marine teleost fish, albeit individual differences in incorporation rates may exist [3,4]. To date, most of the studies measuring otolith $\delta^{18}O$ composition in tropical tuna species (skipjack tuna *Katsuwonus pelamis*, yellowfin tuna *Thunnus albacares* and bigeye tuna *Thunnus obesus*) had been done by isotope ratio mass spectrometry (IRMS). One of the limitations of the IRMS is that relies on obtaining a minimum amount of powder from otolith milling. As a result, the technique does not allow for fine temporal scale resolution (i.e., the signal corresponding to several months must be integrated) or fine scale life history reconstructions (i.e., core to edge transects). As secondary ion mass spectrometry (SIMS) allows to measure stable isotopes at higher spatial/temporal resolution, it might provide a good solution to unravel migration patterns and life history characteristics at much shorter timescales. Our aim was to test the utility of SIMS technique to provide detailed insights into the movements and life history of yellowfin tuna in the Indian Ocean.

For that, a pilot SIMS analysis was performed on one otolith of an adult yellowfin tuna (134 cm fork length) at the NERC Ion Microprobe Facility from the University of Edinburgh. Overall, the SIMS analysis provided a good resolution of $\delta^{18}O$ estimates along the otolith growth transect. In total, 40 spots were analysed along the otolith growth axis from core to edge, spanning fish' life history from birth to death. Otolith $\delta^{18}O$ values measured by SIMS ranged from -2.13 to -0.65 along the growth transect. There was an increasing trend in mean $\delta^{18}O$ values from the otolith core to the edge, corresponding with an increasing in fish age (Fig. 1).

Observed results may indicate that he analysed yellowfin tuna may have spent parts of its life in different water masses. The relatively little $\delta^{18}O$ variability found in the beginning of the transect may indicate retention within a homogeneous area in the first months of growth. At this part of the transect observed $\delta^{18}O$ values were lower, and as fish grew, detected $\delta^{18}O$ values increased. According to the inverse relationship between otolith $\delta^{18}O$ and water temperature [2,5], this suggests an overall decrease in experienced ambient waters temperatures. This trend may reflect a migration from equatorial waters to lower latitudes, a shift in the depth niche inhabited, or more likely, a combination of both.

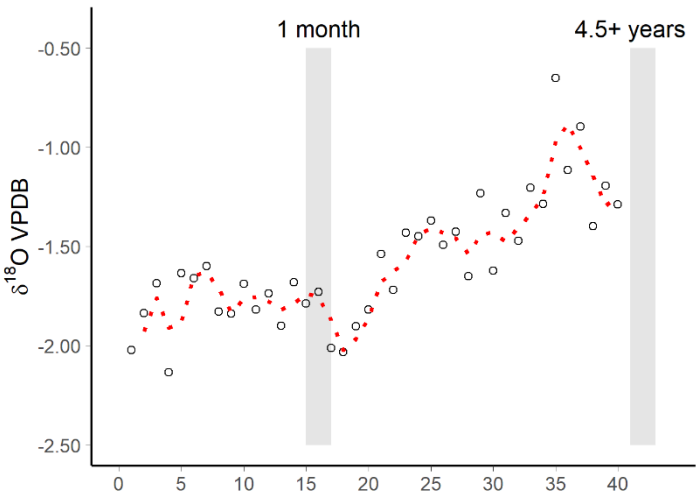

Fig. 1. Core to edge profile of otolith $\delta^{18}O$ values measured by SIMS in an adult yellowfin tuna. Dots are values measured at each spot, and dashed red line represents the mobile mean.

This pilot study shows that measuring variations in $\delta^{18}O$ across an otolith growth axis using the SIMS approach can provide fine scale information of the different environments experience by the fish

over its lifetime, which may be particularly useful for comparing relative patterns of $\delta^{18}O$ composition among contingents, that is, fish with divergent migrations within stocks.

References

[1] T. Kitagawa et al. (2013) Marine Ecology Progress Series 481, 199-209 [2] S. Thorrold et al. (1997) Geochimica et Cosmochimica Acta 61, 2909-2919 [3] A. Darnaude et al. (2018) Marine Ecology Progress Series 598, 167-185 [4] A. Darnaude et al. (2014) PloS One 9, e108539 [5] C.N. Trueman (2012) Journal of Fish Biology 81, 826-847

Appendix: Analytical information

The otolith was first embedded in a rectangular box with two-part epoxy resin (Araldite 2020, Huntsman Advanced Materials, Switzerland). The resultant block was polished from the otolith rostrum using 3M® silicon carbide sandpaper (particle size= 220 µm) and a series of decreasing grain diameter lapping discs (30, 15, 9, 3 and 1 µm) with a lapping wheel, moistened with ultrapure water, until the primordium was exposed. Then, the resin block was then embedded again with the rostrum upwards in a 25 mm diameter silicon cylindric mould with two-part epoxy resin until the surface of the section was covered. It was then kept at a room temperature for 48 h to cure the resin. The obtained cylinder containing the otolith positioned vertically was then polished with a series 3M® silicon carbide lapping discs (9, 3 and 1 µm), moistened with ultrapure water, until the primordium was clearly exposed. A velvet polishing pad moistened with ultrapure water and sprinkled with aluminium powder (0.5 µm) was used to expose the core on a flat mirror-finished surface. The oxygen isotope data were acquired at the NERC Ion Microprobe Facility (SIMS) from the University of Edinburgh with a Cameca IMS 1270, using a ~5 nA primary 133Cs+ beam. Secondary ions were extracted at 10 kV, and 16O- (~3.0 x109cps) and 18O- (~4.0 x106 cps) were monitored simultaneously on dual Faraday cups (L'2 and H'2). Each analysis involved a pre-sputtering time of 60 seconds, followed by automatic secondary beam and entrance slit centring and finally data collection in two blocks of ten cycles, amounting to a total count time of 80 seconds. The internal precision of each analysis is < 0.2 per mil. To correct for changes in the instrumental mass fractionation (IMF), all data were normalised to a UWC-1 (δ18O = 23.3 SMOW) calcite standard which was mounted together with the samples and measured throughout the analytical sessions. The external precision is estimated from the repeat analysis of the standard to be (0.17 – 0.26) per mil). Finally, $\delta^{18}O$ data were converted from VSMOW to VPDB using the following equation:

$$\delta^{18}O_{VPDB} = 0.97001 \times \delta^{18}O_{VSMOW} - 29.99‰ \quad (1)$$

Understanding basaltic Plinian eruptions

E.C. Bamber[1], M.R. Burton[1], M. Polacci[1,] M. Hartley[1], G. La Spina[1], M. de' Michieli Vitturi[2] & F. Arzilli[1]

[1]Department of Earth and Environmental Sciences, The University of Manchester, Manchester, M13 9PL, UK
[2]INGV, Sezione di Pisa, Pisa, 56125, Italy

Motivation

Plinian eruptions are a rare, but highly explosive and hazardous end-member of volcanic activity at basaltic systems. However, the driving mechanisms of basaltic Plinian activity are still debated. To produce an explosive eruption, magma must fragment during ascent within the conduit. For low viscosity basaltic magmas, three fragmentation mechanisms have been proposed: brittle fragmentation, inertial fragmentation and fluid dynamic induced break-up. Ultimately, the eruptive style has important implications for the volcanic hazard.

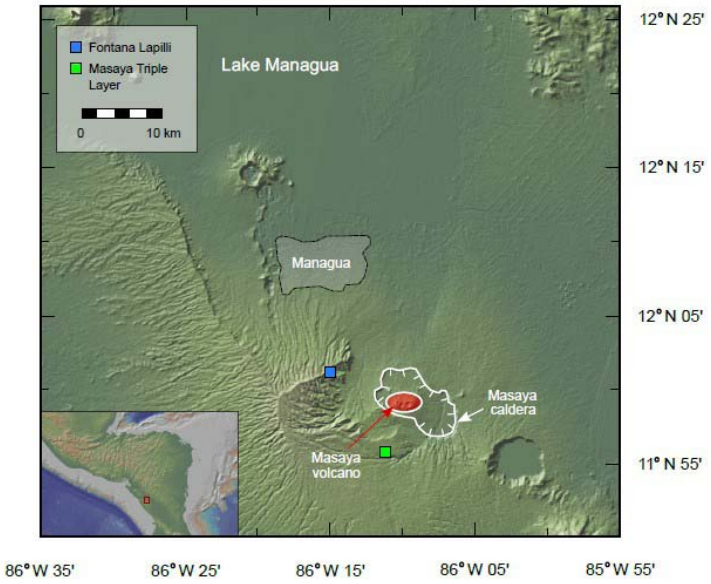

Figure 1: A map of Masaya volcano in western Nicaragua, showing the location of the capital Managua, and sampling localities for the project. Topographic map from [1].

Las Sierras-Masaya volcanic system, Nicaragua, has produced multiple Plinian events over 60, 000-years, including the Fontana Lapilli (60 ka) and the Masaya Triple Layer (2.1 ka) eruptions. In order to understand the driving mechanisms of these eruptions, it is crucial to determine the pre- and syn-eruptive conditions. As volatile exsolution of H_2O and CO_2 drives magma ascent and explosive eruptions, it is crucial to constrain the initial volatile budget. Melt inclusions entrapped within phenocrysts can preserve pre-eruptive volatile concentrations. By measuring stored volatile concentrations we can provide insight into the pre-eruptive condition and assess the relative importance of initial volatile concentrations in driving Plinian activity at this volcanic system.

Samples and methodology

We collected scoria of the Fontana Lapilli and Masaya Triple Layer eruptions during fieldwork in Nicaragua in 2018. Samples are phenocryst poor, with a mineralogical assemblage dominated by plagioclase (7-5 vol.%), with minor clinopyroxene (1-3 vol.%) and olivine (1-2 vol.%). We analysed H_2O, CO_2, F and Cl in 44 plagioclase-hosted melt inclusions and matrix glasses using the Cameca IMS 7f-Geo across two analytical sessions in December 2019 and 2020. Major element chemistry was analysed using the JEOL JXA-8530F at the Photon Science Institute, University of Manchester. This data was then incorporated in the 1-D, multiphase, steady-state conduit model of La Spina et al., (2021) [2] in order to simulate conduit processes.

Results

Table 1 summarises the H_2O, CO_2, F and Cl concentrations measured in melt inclusions of the Fontana Lapilli and Masaya Triple Layer eruptions. Matrix glasses record lower volatile concentrations of 0.1 wt.% H_2O and 0-110 ppm CO_2, reflecting degassing during magma ascent and eruption. Melt inclusions of the Fontana Lapilli eruption record higher volatile concentrations than those of the Masaya Triple Layer eruption. Melt inclusions of Plinian phase Unit E of the Fontana Lapilli eruption record the highest

H_2O and CO_2 concentrations. Volatile concentrations in melt inclusions of units TLL1 and TLL2 of the Masaya Triple Layer eruption overlap.

Eruption	H_2O (wt.%)	CO_2 (ppm)	F (ppm)	Cl (ppm)
Fontana Lapilli *Unit D*	0.9-1.2	100-230	1000-1060	1900-2100
Fontana Lapilli *Unit E*	1.5-2.3	480-1140	820-910	1460-1660
Masaya Triple Layer *TLL1*	1-1.3	170-480	620-950	710-1290
Masaya Triple Layer *TLL2*	1.1-1.2	130-320	660-750	770-1180

Table 1: Ranges of H_2O, CO_2, F and Cl from SIMS analysis of melt inclusions.

Implications

Higher volatile concentrations in melt inclusions of the Fontana Lapilli eruption relative to the Masaya Triple Layer eruption may reflect a temporal evolution of the pre-eruptive condition of Las Sierras-Masaya volcanic system, such as higher pre-eruptive storage pressures. Melt inclusions of the Fontana Lapilli eruption show a small increase in H_2O and CO_2 concentrations over the duration of the Plinian phase. Volatile concentrations measured in melt inclusions from TLL1 and TLL2 overlap. However, TLL1 represents the less explosive, initial phase of the eruption and TLL2 the first Plinian stage of the Masaya Triple Layer eruption [3]. This result suggests that there is minimal change in the pre-eruptive volatile budget for phases of different explosive intensity at Las Sierras-Masaya volcanic system. This result also corresponds with the recent eruptive history of Masaya Volcano, where a maximum H_2O concentration of 1.45 wt.% has been measured in melt inclusions from scoriae of less explosive activity [4]. The consistent low volatile concentrations measured from erupted products at Las Sierras-Masaya volcanic system suggests that the initial volatile concentration may have less importance in driving highly explosive eruptions of this system, and that there may be contribution from other factors such as the degassing path, decompression rate or crystallisation [5]. Preliminary numerical simulations using the conduit model of [2] indicate that an explosive eruption can occur incorporating these measured volatile concentrations.

References

[1] Ryan, W.B.F. et al. (2009) Geochemistry Geophysics Geosystems 10(3). [2] La Spina, G. et al. (2021) Earth and Planetary Science Letters 553, 116658. [3] Pérez, W. et al. (2009) Journal of Volcanology and Geothermal Research 179, 191-205. [4] Zurek, J. et al. (2019) Journal of Volcanology and Geothermal Research 378, 16-28. [5] Bamber, E.C. et al. (2020) Journal of Volcanology and Geothermal Research 392, 106761.

Copper enrichment in arc magmas in Java, Indonesia

N.D. Barber[1], M. Edmonds[1], S. Baldwin[2], F. Jenner[3], H. Williams[1], H.E. Wibowo[4] & A. Harijoko[4]

[1]Department of Earth Sciences, University of Cambridge, UK.
[2]School of Geosciences, University of Edinburgh, Edinburgh EH9 3JW, UK
[3]School of Environment, Earth and Ecosystem Sciences, The Open University, MK7 6AA, UK
[4]Department of Geological Engineering, Universitas Gadjah Mada 55281. Yogyakarta, Indonesia

Background and Rationale

Copper, sourced from porphyry deposits formed in arc settings, is a critical resource for the burgeoning green economy. The processes that shape the copper contents of magmas is well understand in economic geology and are increasingly being investigated in active volcanic settings. Assessing the impact of degassing and water contents on volcanic copper contents is of vital importance in developing a cohesive framework that links modern volcanism with the extinct products of such activity, which we currently mine for metallic resources. To address this need, we use a combination of Raman spectroscopy, SIMS, EMPA, and LA-ICPMS on olivine- and pyroxene-hosted melt inclusions (MIs) from three volcanic centers in Java, Indonesia: Galunggung (West Java), Slamet and its scoria cone Loyang (Central Java), and Bawean (Java Sea) (Figure 1). Java is known to have some of the highest H_2O contents ever measured in olivine-hosted MIs [1], a well-documented and violent history of major eruptions - including a VEI 4 eruption at Galunggung in 1982 and VEI 2 eruption at Slamet in 2014 - and some promising if understudied porphyry prospects (Figure 1; [2]). We made SIMS measurements on a subset of MIs containing a Raman-measurable CO2 signal to better constrain the % degassing in these samples, and to provide a barometric estimate – the hope is that these parameters show systematic trends with copper and other metal contents in these same MIs.

Results and Discussion

A total of 68 SIMS measurements were made on 42 olivine hosted melt inclusions. This forms roughly a quarter of the total number of melt inclusions measurements we intend to make with the remainder of our SIMS time. Each of those melt inclusions were subsequently measured by EMPA and corrected both for post-entrapment crystallization (PEC) [3] and vapour bubble CO_2 density [4]. Figure 2a shows the core composition of those olivine's hosting the melt inclusions – most notable is that discordance between Slamet and its scoria cone Loyang, whose olivine's seem to be sourced from a much more primitive parental melt. Melt compositions were corrected to a 1200 ° C, 3000 bar, +1 delta NNO starting composition, showing a degree of PEC of between 3.7 and 30% (Figure 2b). Figure 2c shows the preliminary volatile data. As EMP measurement shave not been completed, the full 42 melt inclusion suite cannot be shown at this time. Preliminarily, Figure 2c shows two of the Raman-corrected CO_2 measurements, showing a greater than 50% increase in CO_2 where a vapour bubble can be measured. These CO_2 contents at Slamet and Loyang show varied transcrustal magmatic system tapped by both eruptive centres, suggesting the utility of using monogenetic cones to plumb the depths of magma mushes.

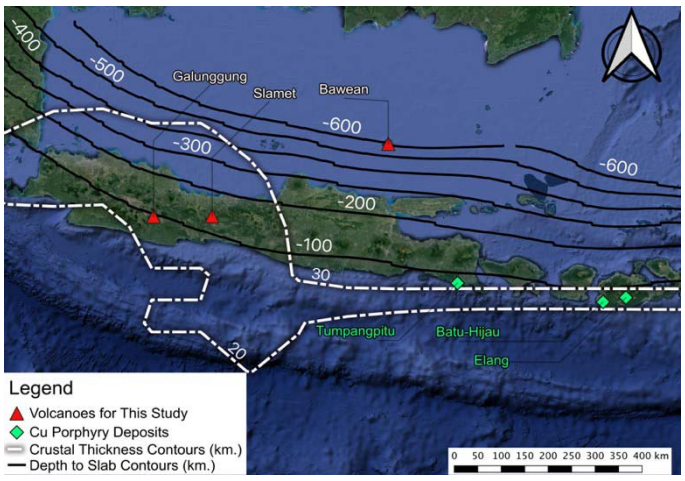

Fig. 1. Map showing the volcanoes (red triangles) from which our samples were collected (Galunggung, Slamet, and Bawean) in Java, Indonesia. Also shown are globally significant Cu porphyry deposits (green diamonds). Slab-depth contours themselves at 100 km intervals in orange. Data from Smithsonian Global Volcanism Program, USGS, [2].

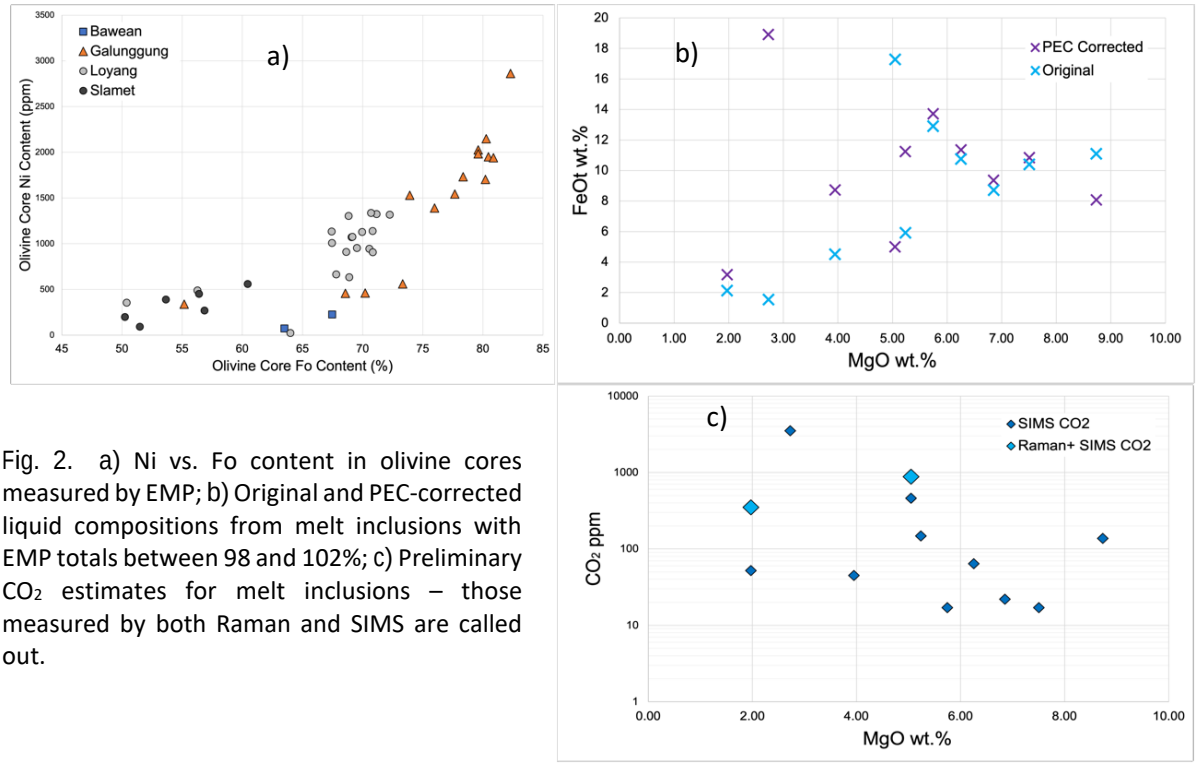

Fig. 2. a) Ni vs. Fo content in olivine cores measured by EMP; b) Original and PEC-corrected liquid compositions from melt inclusions with EMP totals between 98 and 102%; c) Preliminary CO_2 estimates for melt inclusions – those measured by both Raman and SIMS are called out.

References

[1] N. Vigouroux et al. (2012) Geochemistry, Geophysics, Geosystems 13(9). [2] L.D. Setijadi et al. (2006) Resource Geology 56, 267-292. [3] V.C. Kress and M.S. Ghiorso (2004) Journal of Volcanology & Geothermal Research 137, 247-260. [4] P. Wieser et al. (2021) Geochemistry, Geophysics, Geosystems 22, e2020GC009364

Effect of oxygen fugacity and water content on multiple saturation points in oxidised arc magmas: Characterising mantle wedge chemistry beneath Grenada, Lesser Antilles

E. Becerra-Torres[1], E. Melekhova[1,2], J. D. Blundy[1,2] & R. A. Brooker[1]
[1]School of Earth Sciences, University of Bristol, Wills Memorial Building, Bristol BS8 1RJ, UK
[2]Department of Earth Sciences, University of Oxford, UK

Overview

Primitive arc magmas a valuable source of understanding the nature and thermal structure of underlying mantle wedge, and magmatism. Therefore, exploring the effect of water and redox state of island arc basalts can give valuable insights into mantle wedge characterization and their role in arc magmatism.

The Lesser Antilles arc is a slow-rate subduction arc, frequently described as a mature magmatic system. However, the southernmost section, bracketed by Grenada and St. Vincent Islands, present predominantly basalt and basaltic andesite magmatism [1,2], suggesting a more primary stage of magmatism. Lava chemistry of Grenada although being primitive (big proportion of high-MgO basalts) indicates considerable contribution from subducted sediments.

Subduction zone environments tend to produce more oxidized magmas than those produced in extensional environments [3]. The subducted sedimentary layers have been shown to be important contributors of oxidizing agents [4]. Therefore, Grenada primitive basalts an ideal material to experimentally explore the effect of fO_2 and H_2O on the mantle wedge nature and thermal structure [5].

The redox state in experimental assemblages is not an independent variable and volatiles play a significant role in fO_2 of an experiment. For instance, the water dissociation reaction ($H_2O \Leftrightarrow H_2 + 1/2O_2$) combined with hydrogen diffusion out of Au/Pd capsule favor the direct reaction and will lead to oxidation of experimental run. Conversely, diffusion of hydrogen into a capsule favors the inverse reaction and will reduce experimental run. Therefore, it is crucial to analyse experimental run products for H_2O and CO_2.

In this study, we use an inverse experimental approach similar to our study on Mexican basalt [6] to constrain multiple saturation points on the liquidus surface of primitive high-MgO basalt (G507). Equilibrium piston-cylinder experiments were carried out between 0.8 and 2.5 GPa under hydrous conditions (1 - 6.6 wt% H_2O) and a wide range of fO_2 (ΔFMQ +5 to +11).

Results

Volatile contents of 13 experimental glasses were analysed by secondary ion mass spectrometry (SIMS) at NERC ion microprobe facility at University of Edinburgh, using a Cameca IMS 7f-Geo.

Each analysis was preceded by a 2 min presputter with a 15 µm raster of the analytical area to remove surface contaminants. H_2O and CO_2 backgrounds were determined on H and C-free glasses or minerals and amounted to <0.015 wt.% H2O and <20 ppm CO2, and were subtracted from each analysis. H_2O and CO_2 were calibrated against synthetic basaltic glass standard containing ≤4 wt% H_2O and ≤2200 ppm CO_2. Working curves of $^{1}H/^{30}Si$ vs H_2O and $^{12}C/^{30}Si$ vs CO_2 gave straight lines with $R^2 \geq 0.99$.

In Figure 1 we present a liquidus surface diagram for experiments with initial variable H_2O content and melt fraction more than 92 %. In this study we obtained only one experiment were olivine (Fo% 98) coexisting with orthopyroxene (En% 92). This assemblage is stable near liquidus at the lowest investigated pressure and H_2O content. Calculated redox for this experiment is FMQ + 4.6. We found that orthopyroxene has a very extended P-T stability field at the liquidus at oxidized conditions (1.7 to 0.8 GPa, and 1200-175ºC). The pink quadrilateral in Figure 1 illustrates an ol+opx+cpx+sp multiple saturation point defined by 4 experiments between 1250 - 1275ºC and 0.8 - 1.1 GPa. This suggest that

G507 basalt was last equilibrated with the mantle at these conditions if we assume that environment is as oxidised as FMQ + 4.6.

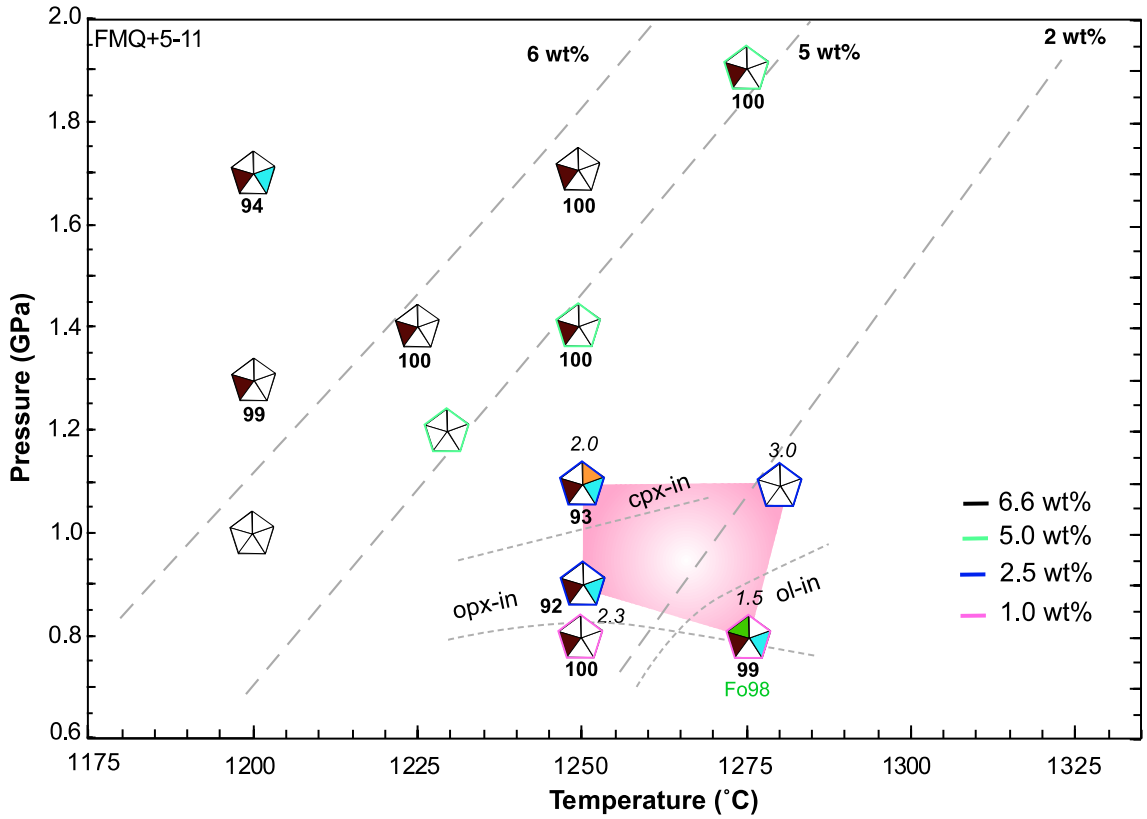

Fig. 1. Liquidus surface diagram for bulk composition G507. Only experiments containing ≥92% glass are plotted. Different outline colours for pentagons represent suite of particular starting water content of each experiment. The number next experiments in italics are melt H_2O content measured (SIMS), in bold the melt fraction obtained by mass balance. Olivine composition, as mol% Fo in green, and Liquidus contours (dashed grey) are labelled with the corresponding H_2O content of the melt. The pink shaded quadrilateral form by the 4 experiments that define a forced MSP at extreme oxidised condition of FMQ +4.6

Discussion

Combining these experiments with MELTs modelling and previous studies on primitive basalts we found that the effect of fO_2 on olivine + orthopyroxene stability is much bigger than effect of H_2O and therefore has a profound influence on generating multiply saturated assemblages.

Grenada olivines have been described as high-Fo ($Fo_{86\text{-}91.4}$). The range of water reported in melt inclusions is in the range of 0.2 to 4.1 wt% H_2O [7]. Using the most forsteritic olivine phenocrysts (91.4) and G507 bulk composition we calculate a Kd of 0.223 (equilibrium constant between melt and olivine). Obtained Kd deviates from a standard $Kd_{Fe\text{-}Mg}$ = 0.30 and demonstrates that a maximum fO_2 for Grenada basalts is FMQ+2 [8]. The experiments presented here lucking olivine on they liquidus not because of incorrect initial H_2O content was chosen for the experiments but because of very high fO_2. Our pMELTS modelling using similar water range used in these experiments and the same starting composition predict olivine on the liquidus at FMQ+2.

References

[1] Melekhova E, Blundy J, Robertson R, Humphreys MCS (2015) J Petr 56:1, 161-192, [2] Stamper CC, Blundy JD, Arculus RJ, Melekhova E. (2014) J Petr 55:7, 1353-1387, [3] Eggins SM (1993) Contrib Miner Pet 114, 79–100, [4] Evans KA, Elburg MA, Kamenetsky VS (2012) Geology 40:783–786. [5] Cooper GF, Macpherson CG, Blundy JD, et al (2020) Nature 582, 525–529. [6] Becerra-Torres E, Melekhova E, Blundy JD, Brooker RA (2020) Contrib Miner Pet 175:101. [7] Bouvier A.-S, Metrich N, Deloule E (2010) G3 11:9. [8] Blundy J, Melekhova E, Ziberna L et al (2020) Contrib Miner Pet 175:103

Volatile concentrations of zircon-hosted melt inclusions from mineralised and unmineralised magmatic systems

D.A. Butters, J.D. Blundy, B.C. Tattitch & C.J. Hawkesworth

School of Earth Sciences, University of Bristol, Bristol BS8 1RJ, UK

Background

Melt inclusions are droplets of melt that become trapped within crystals during their growth from magma. Melt inclusions preserve snapshots of instantaneous melt compositions over the crystallisation interval of the mineral host. The major element, trace element and volatile compositions of melt inclusions are routinely measured using microbeam techniques to understand magmatic processes such as melt fractionation, mixing and assimilation, and for placing constraints on system parameters such as entrapment pressure, temperature and fO_2 [1]. Melt inclusions hosted in olivine, quartz and plagioclase are frequently analysed, however, these primary mineral phases are often altered/destroyed by corrosive magmatic fluids such as those in porphyry copper systems. To bypass this, we measure melt inclusions hosted by the extremely refractory mineral, zircon. Zircon-hosted melt inclusions (ZHMIs) are generally smaller (typically <30 μm) than those in other host phases and are often crystalline requiring homogenisation to a single-phase glass before microbeam analysis. This study aims to ascertain whether volatiles are preserved in homogenised ZHMIs from intrusive ore-bearing and intrusive and extrusive barren magmatic systems.

Samples

Zircons were separated from several porphyry copper intrusions, a barren sub-volcanic intrusive unit and a volcanic extrusive (tuff) unit. Most ZHMIs contained daughter crystals ± volatile bubbles. Crystalline ZHMIs were reheated and quenched to glass at either atmospheric or elevated pressure, before grinding and polishing (Fig. 1). Due to the small size of the melt inclusions, zircons were individually mounted and polished in 3 mm aluminium pips, which were then pressed into indium. Approximately 50 ZHMIs across all samples were analysed for H_2O, CO_2, Cl, F and S using the EIMF Cameca 1270 SIMS instrument. A Cs^+ primary ion beam running at 1 nA was used to collect negatively charged secondary ions. Post-analysis SEM images showed the SIMS pits to be 10 x 10 μm and ~0.5 μm deep.

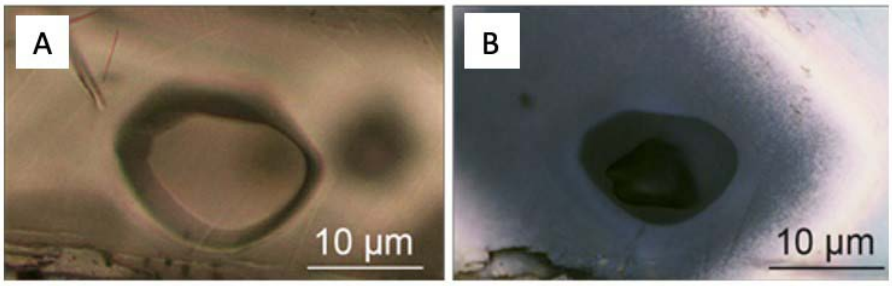

Fig. 1. Polished ZHMI B) Polished ZHMI with SIMS pit and sputtered gold coat.

Results

The major element composition of ZHMIs was measured by EPMA post-SIMS, and SIMS data were normalised to stoichiometric oxygen. All ZHMIs were rhyolitic in composition.

Water is preserved in homogenised ZHMIs

The ZHMIs from the porphyry and subvolcanic intrusive units contain appreciable H_2O contents ranging from 0.7–5.6 wt.% (Fig. 2A). The tuff unit ZHMIs contain very low H_2O (avg. 0.1 wt.%); this could be due to incomplete resorption of H_2O-bearing volatile bubbles during homogenisation at atmospheric pressure or possibly the melt from which the zircons grew was already depleted in H_2O from shallow

system degassing. The H_2O contents of ZHMIs in this study are consistent with those measured in similar investigations [2,3] and suggest that any diffusion of H through the zircon lattice during homogenisation is likely to be minimal.

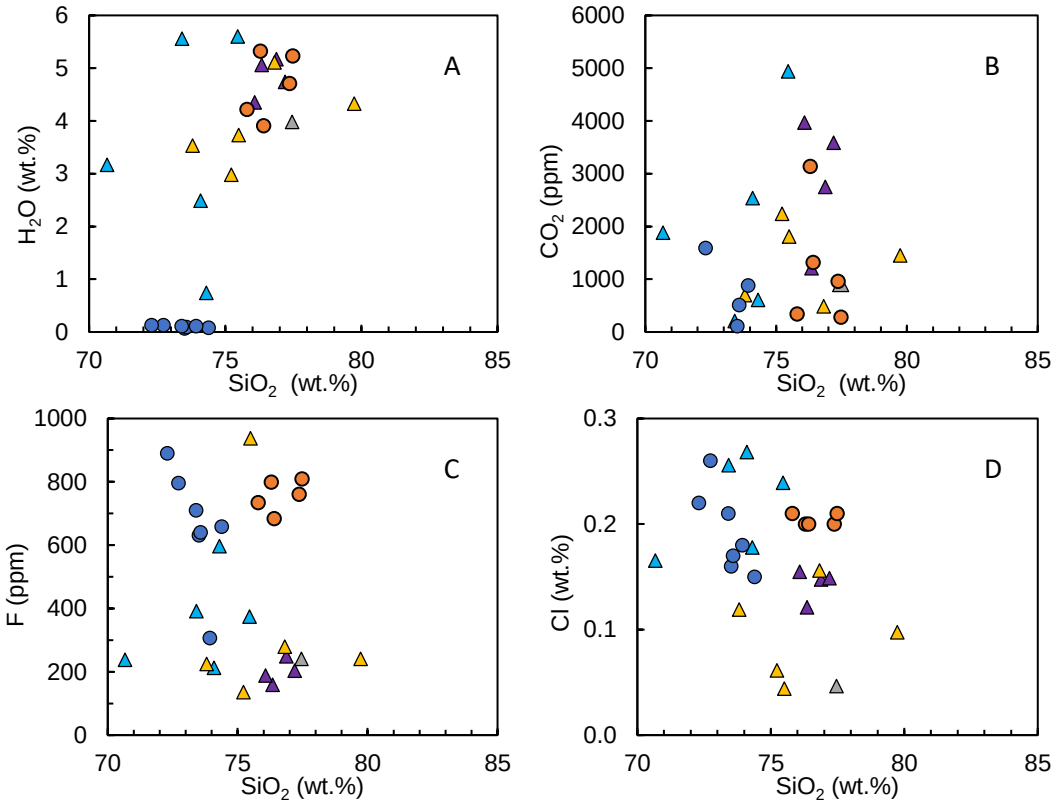

Fig. 2. Harker plots showing ZHMI compositional variability for A) H_2O, B) CO_2, C) F and D) Cl. Triangles are mineralised porphyry copper deposit samples, blue circles represent the tuff unit and orange circles are the sub-volcanic intrusive sample.

The CO_2 content of ZHMIs from mineralised porphyry systems is greater than in the barren systems

The CO_2 budget of primary porphyry melts is poorly constrained; however, we have used ZHMIs to directly analyse CO_2. The CO_2 content of the porphyry ZHMIs ranges from ~200–5000 ppm, whereas CO_2 in the barren tuff and intrusive samples is typically <1500 ppm (Fig 2B). The elevated CO_2 in porphyry ZHMIs is interpreted to reflect greater pressures and thus depths of entrapment in comparison to the other samples. This work highlights the significant role that CO_2 may play in the evolution of porphyry melts and that ZHMIs, through H_2O-CO_2 solubility relationships, present effective geobarometers in systems where pressure estimates are otherwise unobtainable.

Fluorine, chlorine and sulphur budget

The F contents of most porphyry ZHMIs are significantly lower (avg. ~300 ppm) than the barren tuff and intrusive samples (avg. ~700 ppm) (Fig. 2C); this suggests that the porphyry melts are less evolved and/or reflect lower degrees of crustal contamination. The Cl contents of the unmineralised samples are generally higher (~0.2 wt%) in comparison to the other porphyry ZHMIs (<0.15 wt%) aside from one porphyry sample with elevated (avg. 0.22 wt%) Cl (Fig. 2D). The latter could be due to zircon growth in a relatively undegassed melt (before significant fluid exsolution). Concentrations of S are low (<100 ppm) in all samples and suggest that porphyry melts are not S-enriched.

References

[1] Blundy and Cashman, (2008) Rev. Min. & Geochem. 69(1), 179–239. [2] Gudelius et al. (2020) GCA, 289, 158–181. [3] Watts and Mercer, (2020) GCA, 272, 54–77.

Tracing subducted volatile fluxes through halogen abundances in the leading edge of the mantle wedge

E. J. Carter[1,2] & B. O'Driscoll[1]

[1]Department of Earth and Environmental Sciences, University of Manchester, Oxford Road, Manchester M13 9PL, UK
[2]Department of Geology, Trinity College Dublin, Dublin 2, Ireland

Background and rationale

Subduction of oceanic lithosphere represents a first-order coupling of the surface and interior of the Earth. The subduction process forms a key part of the geochemical cycles of many volatile elements including carbon and the halogens, with wider implications for global climate and long-term ocean salinity, respectively [1]. Establishing the magnitude of any flux into the deep Earth requires evaluating mass balance between inputs to the subduction system – via altered oceanic lithosphere – and outputs – via slab dehydration and arc volcanism. The magmatic complexities of arc volcanism make quantification of the fluxes associated with dewatering of the slab problematic [2]. In addition, much of the shallow mantle wedge is not sampled by volcanism, potentially leading to "hidden" outfluxes. Estimates of volatile fluxes to the mantle are, as a result, highly uncertain. Ophiolites can help to resolve these issues. They comprise oceanic lithosphere tectonically uplifted during plate collisions. Most ophiolites in the geological record have undergone processing above subduction zones during their emplacement and provide evidence for metasomatism of the mantle wedge by percolating melts or fluids [3].

Samples and geological setting

The ~96 Ma Semail Ophiolite, Oman, is the largest known and best studied ophiolite in the world. The basal thrust of the ophiolite tectonically juxtaposes mantle peridotites on top of metasediments and metabasalts, together interpreted as remnants of the shallow parts of a subduction zone. In places, the basal thrust is overlain by mantle peridotites which have undergone complete carbonation to form listvenites – unusual rocks consisting principally of magnesite ($MgCO_3$) and quartz (SiO_2). It has been suggested that these formed at shallow subduction levels, at temperatures of 100-200°C, through metasomatism by CO_2-rich fluids derived from the downgoing plate [4]. The basal thrust section has recently been sampled by diamond core drilling, as part of the Oman Drilling Project (International Continental Drilling Program expedition 5057). This unique core affords almost complete preservation across a reaction front between the serpentinite protolith (hydrated peridotite) via progressively altered "ophicarbonates" into listvenite (carbonated peridotite). The interval shows a sharp compositional gradient over which external factors such as protolith heterogeneity or later alteration will be minimised and the dominant variation should be due to increasing influence of the carbonating fluid.

The principal aim of this project is to test the hypothesis that fluids derived from subducting sediments are the source of CO_2-rich fluids. If confirmed this would suggest carbonation at the leading edge of the mantle wedge may be a significant and overlooked part of the global carbon cycle. If a component derived from the subducting slab is identified, we further aim to reconstruct the halogen signature of slab fluid(s) to better understand their fluxes from the slab at intermediate subduction depths.

Results and preliminary interpretation

92 point analyses of Br and I were made in serpentine, supplementing the dataset of F and Cl in serpentine and carbonate collected in Autumn 2019. It was not possible to measure Br and I in carbonate due to low concentrations and the lack of a reliable peak-centering species. Bromine and I were determined adjacent to the F-Cl pit using petrographic images and EPMA maps to ensure the second pit was, as far as possible, within the same grain/mineral domain as the as the first. Heavy

halogen concentrations in serpentine were typically 300-2000 ppb Br and 20-200 ppb I and were positively correlated with each one another and with Cl. Plotted together, Br/Cl and I/Cl ratios form a correlated array, collinear with the composition of average sedimentary pore fluid, suggesting this is a major source for these volatiles during carbonation. Seawater, meanwhile, does not appear to have been a significant fluid endmember. In contrast to F, which showed large variation independent of Cl concentration (Fig 1a), the bulk of the variation in I/Cl, and particularly Br/Cl, can be explained by addition or loss of Cl (mediated by contrasting compatibilities of I and Br vs Cl in carbonate) rather than variable fluid chemistry (Fig 1b-d). This implies that either the bulk of the Br and I were supplied by a single fluid, or that the two fluids indicated by the F and Cl data had very similar Br/I ratios.

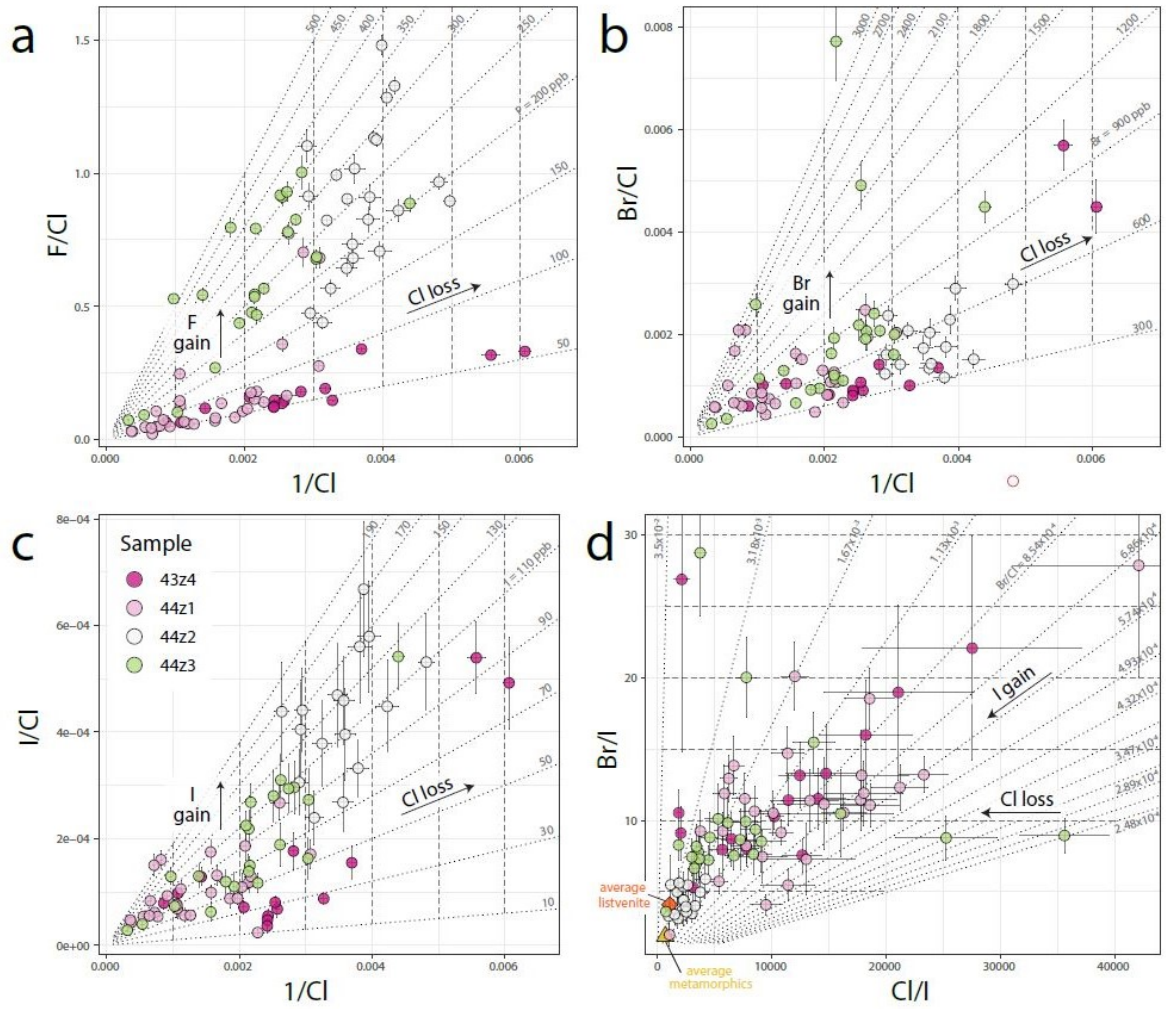

Fig. 1. Halogen relative abundance graphs for serpentine in samples 43z4 (serpentinite)-44z3 (partially-carbonated). Calculated vectors are plotted for Cl loss/gain (fractionation control) and addition of F, Br or I (source control). Variation in Cl abundance alone results in an array along a single Cl loss vector. Variable addition of F, Br or I results in scatter between these vectors.

References

[1] Kelemen et al. (2011) Annual Reviews of Earth and Planetary Science 39, 545–576; [2] Hilton, Fischer and Marty, 2002. Reviews in Mineralogy and Geochemistry 47, 319–370; [3] Dilek & Furnes (2014) Elements 10 (2), 93–100; [4] Falk & Kelemen (2015) Geochimica et Cosmochimica Acta 160, 70–90; [5] Kendrick (2012). Chemical Geology, 292-293 (Jan 2021), 116-126; [6] Marks, et al. (2017) Geostandards and Geoanalytical Research, 41 (1), 107-122; [7] Myers et al. (1976). USGS Tech. Rep; [8] Jochum, et al. (2005). Geostandards and Geoanalytical Research, 29 (3), 285-302

Investigating the fossilisation and nature of sulfur metabolisms of microbes associated with ancient vent animals: tracing sulfide oxidation using $\Delta^{33}S$

M.N. Georgieva[1], C.T.S Little[2], R.J. Herrington[3] & A.G. Glover[1]

[1]Life Sciences Department, Natural History Museum, London SW7 5BD, UK
[2]School of Earth and Environment, University of Leeds, Leeds LS2 9JT, UK
[3]Earth Sciences Department, Natural History Museum, London SW7 5BD, UK

Background

Symbioses between metazoans and microbes involved in sulphur cycling are integral to the ability of animals to thrive within hydrothermal vent environments – the development of such symbioses is regarded as a key adaptation in enabling animals to successfully colonise vents. In order to understand therefore how various animal lineages have evolved to occupy vents throughout geological time, it is crucial to understand how they might have interacted with microbes.

The main isotope of sulphur (^{34}S) is commonly employed to explore the metabolic pathways of organisms from both modern and ancient settings where sulphur cycling can occur [1–2]. While sulphate reduction by microbes usually results in large fractionations, whereby sulphides are depleted in ^{34}S by 10-40‰ compared to seawater sulphate [3], the effects of sulphide oxidation are less clear. At hydrothermal vents, it is especially important to be able to detect sulphide oxidation as it is a crucial driver of primary productivity within vent environments. Recent studies have demonstrated that ^{33}S can be used to trace the occurrence of sulphide oxidation, showing that small changes in $\Delta^{33}S$ are indicative of chemolithotrophic sulphide oxidation [1]. $\Delta^{33}S$ values can also be used to indicate the degree of post-depositional reworking with other distinct sulphur sources [4].

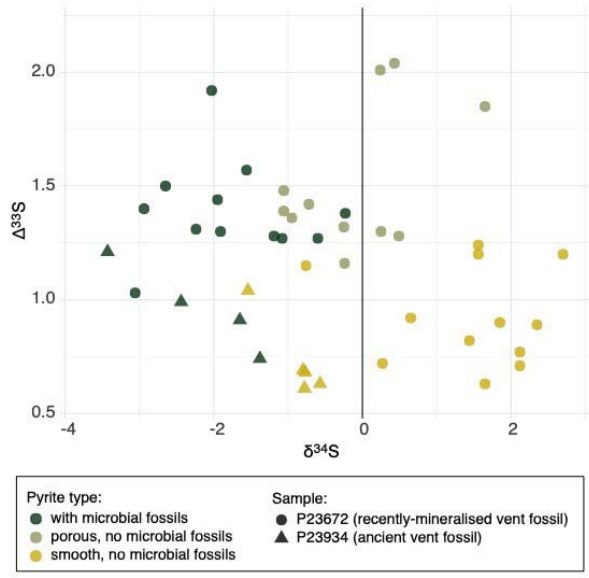

Fig. 1. Results of $\Delta^{33}S$ pilot analyses of recently-mineralised and ancient fossil worm tubes from hydrothermal vents.

Using well-characterised samples for which we have $\delta^{34}S$ data indicative of microbial processing for both modern recently-mineralised and ancient fossil worm tubes, we measured $\Delta^{33}S$ to explore the contribution of sulphide oxidation to observed $\delta^{34}S$ measurements. Specifically, $\Delta^{33}S$ sulphur isotopic data were intended to test the hypothesis that pyrite preserving hydrothermal vent microbes has a $\Delta^{33}S$ signature indicative of sulphide oxidation by chemolithotrophic microorganisms.

Results and Interpretation

In total during the one-day pilot session, we obtained 44 corresponding measurements of $\Delta^{33}S$ and $\delta^{34}S$ (Fig. 1). The points were characterised by pyrite texture type, and show a small but intriguing $\Delta^{33}S$ difference between pyrite that contains microbial fossils, and smooth pyrite that does not. However, our $\Delta^{33}S$ results are about an order of magnitude outside of what would be expected for modern and Silurian hydrothermal vent environments, and we suspect that this discrepancy may be due to the standards that were used for the analyses, for which $\Delta^{33}S$ is not well characterised. If possible, we hope to repeat these measurements using an improved suite of standards.

References

[1] A.L. Zerkle et al. (2016) *Geochim. Cosmochim. Acta* 173, 373-386. [2] R.D. Vetter and B. Fry (1998) *Mar. Biol.* 132, 453-460. [3] Y. Shen et al. (2001) *Nature* 410, 77-81. [4] A. Galić et al. (2017) *Chem. Geol.* 449, 135-146

(page intentionally left blank)

Insights into the residency and behaviour of nitrogen in subduction zones

B.J.R. Harris[1], J.C.M. De Hoog[1] & R. Halama[2]

[1]School of GeoSciences, University of Edinburgh, Edinburgh EH9 3FE, UK
[2]School of Geography, Geology and the Environment, Keele University, Keele, ST5 5BG, UK

Introduction

The Earth's atmosphere is presently composed of 78% nitrogen and is essential for the habitability of the planet. There is considerable debate over the long term evolution of the mass of N in the atmosphere [1] and it is therefore necessary to quantify the flux of N between the surface and the mantle. Subduction zones are the primary locations for return of N from the surface to the mantle but data to constrain this flux are limited, and estimates of this flux are uncertain (Fig. 1).

Nitrogen exists most commonly as ammonium (NH_4^+) in silicate minerals, substituting for K due to its similar ionic size. White mica (predominantly phengite) is the main K-bearing phase at HP conditions in a wide range of lithologies and is critical in controlling the N budget of deeply subducted rocks [2]. Phengite is also a major host of water and fluid-mobile elements, including alkalis, boron and halogens. The behaviour of phengite during subduction is therefore thought to be a dominant control on the recycling of volatile elements, but studies detailing the role of phengite remain surprisingly scarce.

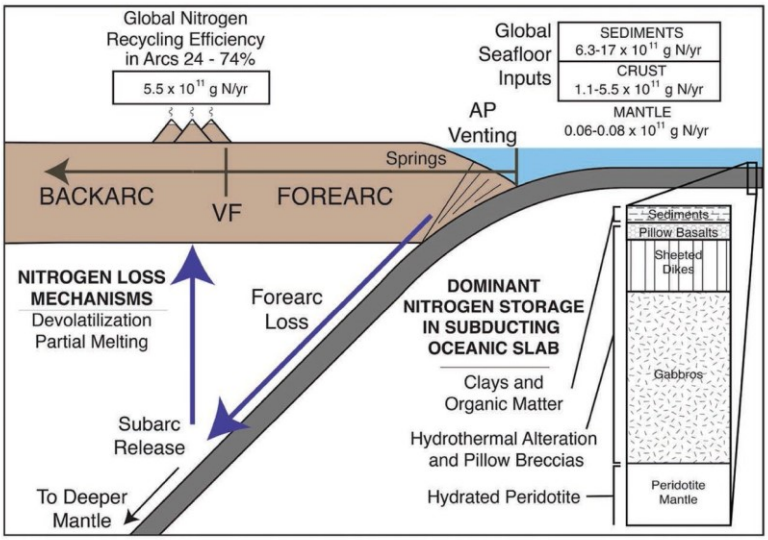

Fig. 1. Overview of the subduction nitrogen cycle [3] showing the large uncertainty in the recycled subduction flux. The extent of forearc loss and subarc release are poorly known, and nitrogen contents of subducted continental crust are currently unconstrained.

This study aimed to determine *in situ* N abundances and variability of white mica and co-existing minerals in subduction zone rocks, and investigate the role of phengite in the behaviour of N during HP fluid-rock interaction by combining N content data with textural information (zoning patterns in minerals, N contents of protolith vs. metasomatic minerals).

Samples

15 samples from four localities were analysed to address our objectives. Three localities (Lago di Cignana, Italy, Raspas, Ecuador and Jenner, USA) represent subduction of oceanic crust, with varying degrees of fluid-induced overprint at different points during the subduction cycle. Samples from Dora Maira (Western Alps, Italy) represent various stages in the subduction of continental crust. A localized metasomatic event occurred at ~ 540 °C, 2.5 GPa, forming whiteschist by metasomatism of the metagranite and orthogneiss country rock.

Results and discussion

White mica is the main host of N, hosting over 75% of the nitrogen in all samples, and over 95% in all

but two samples. Bulk N contents reconstructed from white mica concentrations and modal abundances agree well with measured bulk N contents, where these data are available. Clinopyroxene, glaucophane, epidote and titanite all contain <5 ppm N, and coexist with white micas containing 60-300 ppm N. Matrix chlorite in a blueschist from Jenner contained 10-83 ppm N, coexisting with phengite (108-270 ppm N). This suggests that chlorite may have a previously unrecognised role as a host of nitrogen, but more work is required to analyse the N contents of chlorite in other samples.

Dora Maira samples, representing subducted continental crust, show generally lower nitrogen contents in phengite than the oceanic rocks, but have higher phengite modal abundances. Metapelite has estimated bulk N contents of 26 ppm, which is low compared to previously analysed oceanic metapelites from formerly subducted settings. Orthogneiss contains biotite but we were not able to successfully reproduce N concentrations for our biotite standard, which precluded a comparison of N between the whiteschist and its orthogneiss protolith.

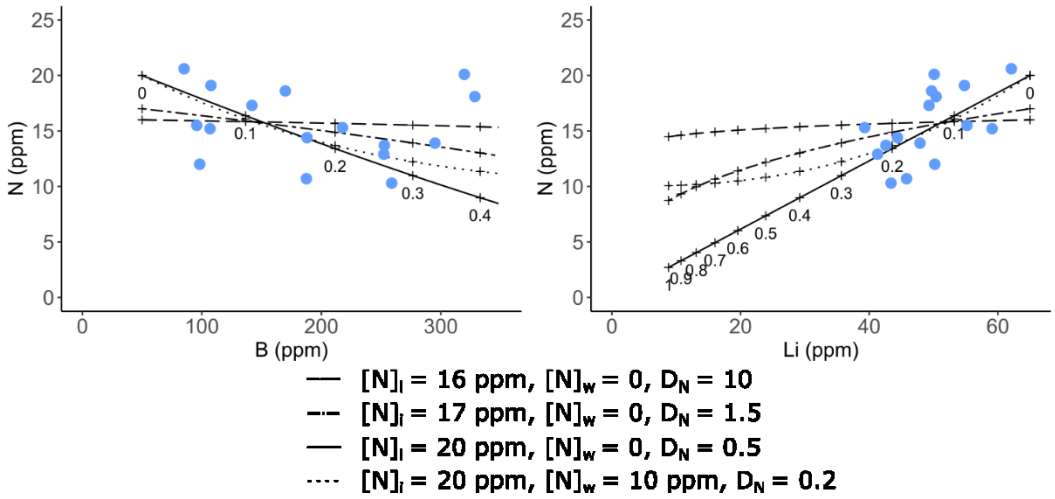

Fig. 2. Open system fluid-rock interaction modelling of garnet-phengite quartzite (LC-3). We vary the phengite-fluid partition coefficient for N (D_N) and show that, in order to fit the trends observed, D < 1.5 is required.

Two samples were investigated in detail to explore the behaviour of nitrogen during fluid-rock interaction. A garnet-phengite quartzite (metachert) from Lago di Cignana shows correlations of nitrogen in phengite with boron and lithium, with nitrogen being lost during fluid-rock interaction. Using numerical modelling to compare to these elements, we were able to constrain the phengite-fluid N partition coefficient to be around 1 (Fig. 2), which is lower than some previously proposed values. A blueschist from Raspas showed evidence for paragonite growth during interaction with a CO_2-bearing fluid. This resulted in redistribution of N between existing phengite new paragonite, with no bulk N loss. This illustrates that the stability of white mica during fluid-rock interaction exerts a strong control on the retention or loss of N.

These data demonstrate the viability and utility of N analyses by ion microprobe. They confirm white mica as the primary host for N in a range of lithologies. They also provide useful constraints on the fluid-mica partitioning behaviour of N in natural samples, which help to constrain models of subduction zone dehydration.

References

[1] Bebout et al. (2013) Elements 9, 333-338. [2] Halama R et al. (2017) Int Geol Rev 59, 702-720. [3] Bebout et al. (2016) Am Min 101, 7-24

Magmatic processes and eruption variability at Mount Taranaki, New Zealand

T. Olver[1], R. Brooker[1] H. Mader[1] & G. Kilgour[2]

[1]School of Earth Sciences, University of Bristol, Bristol BS8 1QE, UK
[2]GNS Science, Wairakei, Taupo, NZ

Rationale

Mt. Taranaki is an unusually high K-andesite stratovolcano in New Zealand, positioned far behind the main focus of subduction related activity, the Taupo Volcanic Zone (Fig.1.). Since 180 k.a, Taranaki has followed catastrophic cycles of dome growth, explosive eruption and near-complete collapse. Throughout the Holocene, 1500-year cycles in andesitic activity at the summit are evident (eruptive episodes), until the formation of a basaltic satellite cone, Fanthams Peak (3.3 – 1 ka) [1]. Since 1 ka, andesitic activity has resumed at the summit, and Fanthams Peak has remained dormant.

Over 100,000 people and critical infrastructure are located on the surrounding Peninsula, meaning a large eruption would likely cause extensive impacts on a regional and national scale. Although an excellent stratigraphic record has been established for Holocene events, studies of the magma system are generally limited to bulk rock and mineral analysis. Relatively little work has been done in attempts to understand the structure of the magmatic plumbing system or to establish eruptive timescales.

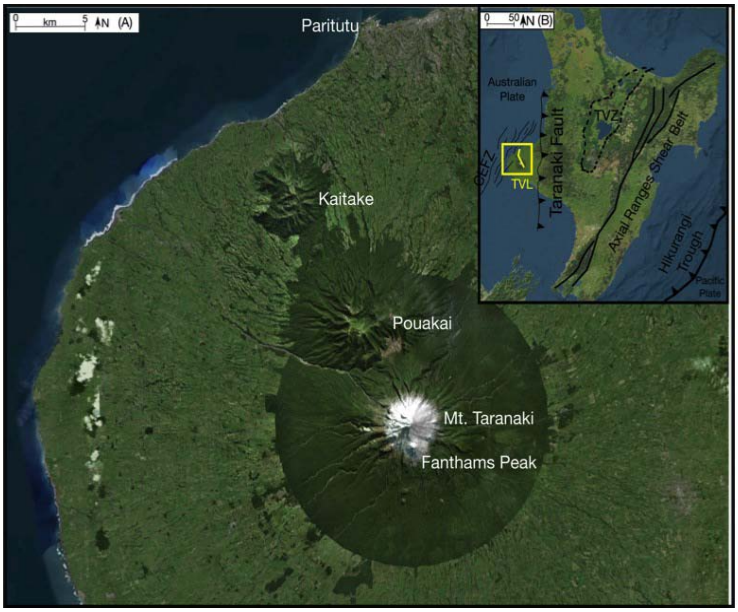

Fig.1. (a) Satellite map of the Taranaki Peninsula highlighting the Mt. Taranaki and Fanthams Peak relative to the older volcanoes on the Taranaki Volcanic Lineament. (b) Highlights the position of the TVL relative to the Hikurangi Trench and Taupo Volcanic Zone, North Island, New Zealand.

Objectives

Due to the hydrous nature of Taranaki magmas, phase-equilibria experiments are required to develop understanding of magmatic evolution and storage. This project will utilise phase-equilibria experiments to understand evolution and pre-eruptive storage conditions of key eruptive episodes, which will be used to inform possible monitoring signals prior to the next eruption. Accurate pressures and temperatures which can be established through analysis of H_2O and CO_2 contents of melt inclusions, are required to constrain the experimental program. Establishing the depth where precursor signals might be found may justify more targeted seismic coverage. Trace element analysis will aid in constraining variations in parent magma compositions and magmatic evolution.

Key units from two Holocene eruptive episodes were selected for initial analysis, the 3.3 ka, andesitic Upper Inglewood episode, which erupted from the summit vent, and the 3.3-1 ka Manganui episode

which erupted from a large satellite cone, Fanthams Peak. Although these events occurred within a relatively small timeframe, activity occurred at two different vents, and the products of which are compositional endmembers relative to other Holocene deposits.

Results and Preliminary Interpretation

Melt inclusions were prepared for analysis at the University of Bristol, and then analysed by Cees-Jan de Hoog at the Ion Probe Facility, due to COVID-19 restrictions.

Isobars based on magma volatile contents were generated in MagmaSat to estimate pressure of entrapment [2]. Early estimated of H_2O and CO_2 saturation pressures (Fig.2.) highlight a potential degassing pathway in the basaltic Manganui melts, from deep within the magma system. The Inglewood melt inclusions suggest that magmas rose from a shallower depth, which would be expected of the andesitic bulk rock and rhyolitic melt compositions.

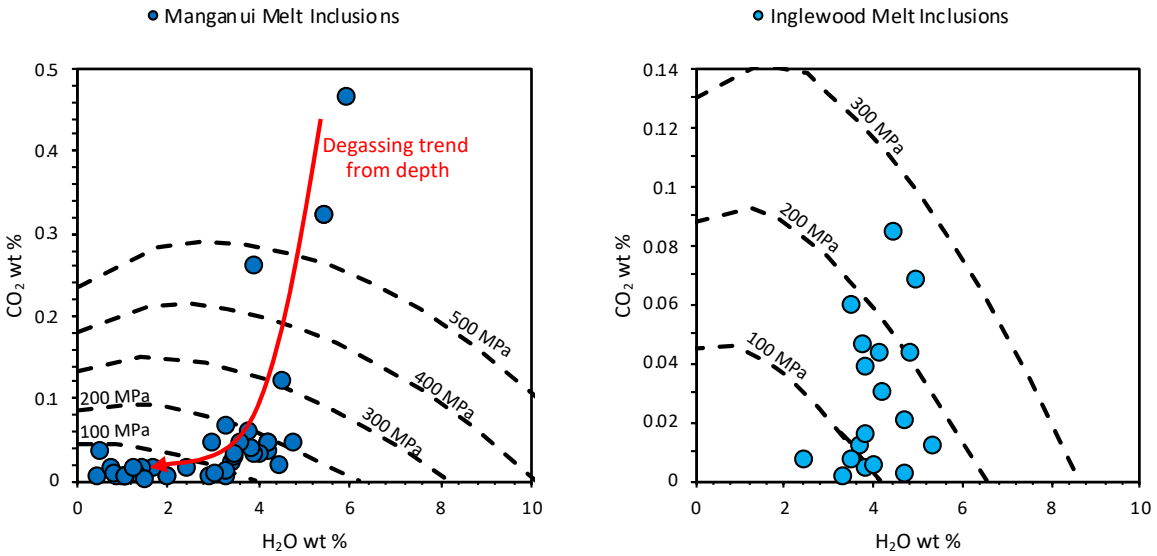

Fig.2. Isobars created in MagmaSat [2] model for a representative (A) Manganui and (B) Inglewood melt inclusion composition, plotted alongside all analyses each sample set. The Manganui Isobars were established using T = 1000°C and the Inglewood T = 900°C.

In addition to these analyses, a sample containing phenocryst hosted melt inclusions from tephra produced during the Burrell eruptive episode has been prepared from analysis. The Burrell was an andesitic event at the summit vent at 1 k.a, after activity had ceased at Fanthams Peak. This will allow for direct comparison with andesites that erupted prior to the Manganui magma (the Inglewood) and test for potential relationship between the events.

References

[1] R. Torres-Orozco et al. (2017) Bull Volcanol 79, 76. [2] M.S. Gualda and G.A.R. Ghiorso (2015) Contrib Mineral Petrol 169, 52

Sulfur cycling at subduction zones: sulfur isotopes in melt inclusions from four Central American volcanoes

Z. Taracsák[1], T.A Mather[1], T. Plank[2], S. Ding[2], D.M. Pyle[1]

[1]Department of Earth Sciences, University of Oxford, Oxford OX1 3AN, UK
[2]Lamont-Doherty Earth Observatory, Columbia University, Palisades NY 16094, New York, USA

Background and Motivation

The Central American Volcanic Arc (CAVA) is among the most active and studied volcanic arcs on the Earth. Located along the active margin of the Cocos and Caribbean Plates, it is built up by >30 volcanic centres that together form a 1100 km long volcanic front close to parallel with the Pacific coast (Fig. 1/A). The CAVA was chosen as a natural laboratory for our first $\delta^{34}S$ melt inclusion study as part of the NSFGEO-NERC "Sulfur Cycling in subduction zones" project as melt inclusion volatile element and volcanic gas emission data are available from many volcanic centres in the arc. Three volcanoes that sample most of the geochemical variability observed along the CAVA were selected for our initial work: Fuego, Cerro Negro, and Turrialba (NW to SE, Fig. 1). The magmas erupted from Cerro Negro and Turrialba volcanoes encompass the maximum and minimum Ba/La ratios along the arc, respectively. Incompatible trace elements (indicated by La/Yb) are most enriched at Turrialba along the arc. The Ba/La ratio thought to increase with slab fluid input into the mantle wedge, and correlates broadly with the H_2O contents estimated for CAVA primary magmas [1] and the CO_2/S ratio of high-temperature volcanic gases [2]. Using in-situ sulfur isotope ratio analyses of melt inclusions (MIs), coupled with volatile concentration analyses, we aim to trace fluid input from the subducted slab into the mantle wedge and determine whether we can distinguish the addition of oxidised (expected to be ^{34}S-rich) or reduced (^{32}S-rich) sulfur species to the mantle source of CAVA magmas.

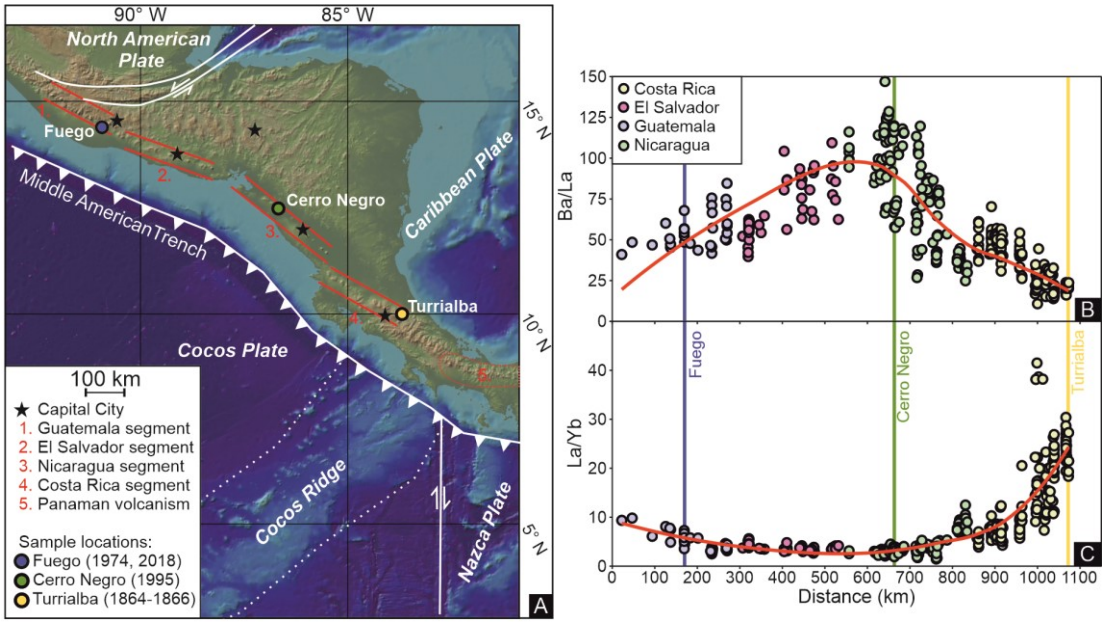

Fig. 1. Map of the CAVA (A) showing the three volcanic centres included in this study. Three out of the four volcanic segments are covered by this work. Furthermore, the three centres cover most of the trace element variability along the arc, including that observed in Ba/La (B) and La/Yb (C) ratios [3].

Preliminary results

As part of this project we measured the volatile and light element content (H_2O, CO_2, F, S, Cl, Li and B) and sulfur isotopic composition of MIs, embayments and matrix glasses from Cerro Negro (1995 eruption, 20 samples), Fuego (1974 and 2018 eruptions, 18 samples) and Turrialba (1865-1867

eruption, 8 samples) using the Cameca IMS-1270 instrument (Fig. 2). Ten MIs out of the 46 glass samples (three from Fuego and seven from Cerro Negro) were re-homogenised experimentally to resorb the vapour bubble common to most MIs. This allowed us to test if volatile-loss to vapour bubbles influence measured S isotope ratios. Due to Covid-19 restrictions we only have been able to collect sulfur isotope and volatile data from the inclusions; light element and further H_2O and CO_2 analyses from the samples are outstanding. We measured up to -5‰ instrumental mass fractionation (IMF) during $\delta^{34}S$ analyses using eight standards containing between 500-3400 ppm S. Work is ongoing to quantify matrix effects observed during analyses.

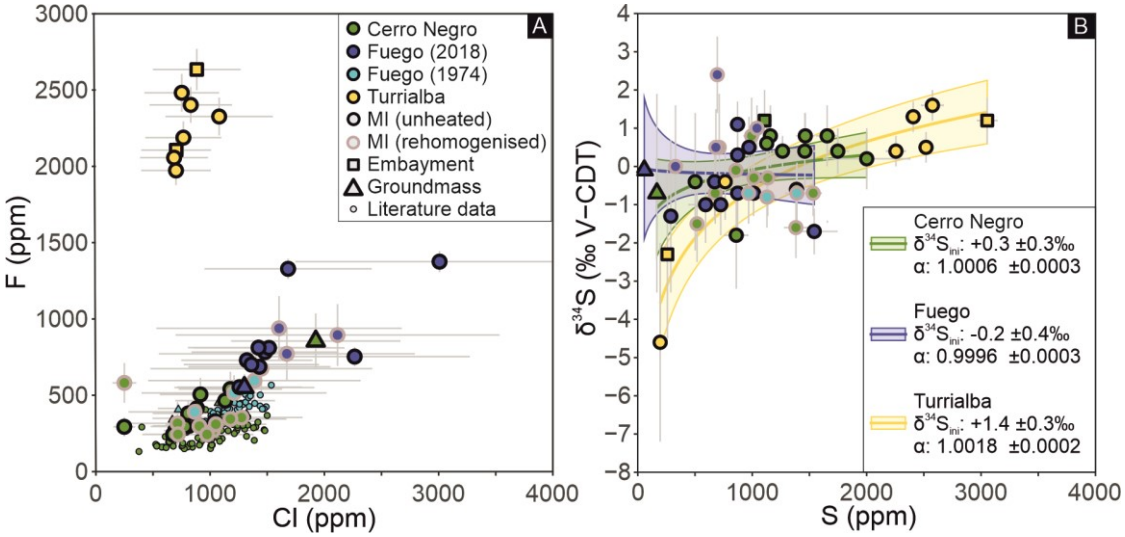

Fig. 2. Fluorine vs. Cl content (A) and sulfur isotopic composition of vs. sulfur content (B) of samples. Sulfur isotope ratios have not been corrected for IMF. Solid lines in (B) indicate open system degassing models fitted between $\delta^{34}S$ and S content, while shaded areas indicate the error of the fitted models (95% confidence intervals). Errors presented in the legend on initial $\delta^{34}S$ and fractionation factors (α) for each volcanic centre are residual standard errors of regression. Error bars are 2σ (using internal precision for $\delta^{34}S$).

Results indicate both undegassed S contents and F/Cl ratios are higher in Turrialba magmas than at the other two centres (Fig. 2/A). Elevated F contents, which is accompanied by elevated rare earth element contents, of Turrialba magmas and others in this portion of the Costa Rican segment of the arc are thought to reflect the subduction of Galapagos-derived volcaniclastic sediments at the Cocos Ridge [4]. Our S isotope fractionation factor estimate between gas and melt for Turrialba is higher (1.002) than for Fuego or Cerro Negro (around 1.000), which is supported by the ^{34}S-enriched composition of Turrialba gases (+7‰, [5]) compared to those emitted at Cerro Negro (+3‰, [6]), as degassing of ^{34}S-rich gases will cause a more prominent decrease in the $\delta^{34}S$ value of degassed Turrialba melts. Sulfur content and $\delta^{34}S$ data in homogenised and un-homogenised Cerro Negro and Fuego inclusions broadly overlap, indicating no significant S loss to bubbles occurred post entrapment. Naturally quenched inclusions are sufficient for studies involving S and its isotopes. Modelling S isotope composition of undegassed magmas result in a primary melt $\delta^{34}S$ estimate of -0.2±0.4‰, +0.3±0.3‰, and +1.4±0.3‰ for Fuego, Cerro Negro, and Turrialba, respectively. Our preliminary results indicate Turrialba primary melts may be more enriched in ^{34}S compared to Fuego and Cerro Negro melts. Cerro Negro and Turrialba display undegassed melt $\delta^{34}S$ that is elevated compared to depleted upper mantle (-0.9 to -1.3‰ [7]), with increasing $\delta^{34}S$ values towards the southwest of the arc.

References

[1] Sadofsky et al. (2008) Contributions to Mineralogy and Petrology 155, 433-456. [2] Aiuppa et al. (2014) Earth and Planetary Science Letters 407, 134-147. [3] Carr et al. (2007) Earth and Planetary Science Letters 8(6), Q06001. [4] Benjamin et al. (2007) Journal of Volcanology and Geothermal Research 168, 68-92. [5] Alfonso et al. (2015) Goldschmidt2015 Abstracts, 43.. [6] De Moor et al. (2013) American Geophysical Union Fall Meeting 2013 Abstract, V41E-07D. [7] Labidi et al. (2013) Nature 501, 208-211.

Arc detection at the cavity couplers of the European spallation source

N. Turner & R. Edgecock

School of Computing and Engineering, University of Huddersfield, Huddersfield HD1 3DH

The European Spallation Source (ESS) is a high brightness source of slow neutrons which is currently under construction in Sweden [1]. Arc detection is required to protect the cavity couplers of the ESS [2] from the potential consequences of electrical discharges [3]. Multimode optical fibres [4] have been proposed as the medium for transmitting light from incipient arcs in the cavity couplers to detection electronics.

The University of Huddersfield is investigating the optical transmission and radiation resistance properties of a range of multimode optical fibres, including assemblies of 70 micron diameter Schott glass filaments. Details of the composition of the glass optical filament are not provided by the supplier. The Edinburgh University Ion Microprobe Facility provides a means for investigating the composition profile of the filaments.

References

[1] R. Garoby (2018) Physica Scripta, 93, 014001.
[2] C. Darve et al. (2014) AIP Conference Proceedings, 1573, 1, 639-646.
[3] Y. Saito (1995) IEEE Transactions on Dielectrics and Electrical Insulation, 2, 2, 243-250.
[4] A. W. Snyder (1969) IEEE Transactions on Microwave Theory and Techniques, 17, 12, 1138-1144.

(page intentionally left blank)

Utilising SIMS to determine the Br and I content of basaltic glass

E. Waters & M. Hartley

Department of Earth and Environmental Science, University of Manchester, Manchester, M13 9PL, UK

Aims of project

Halogens are concentrated in oceanic crust and are released into the mantle following subduction, making them potentially excellent tracers of recycled subducted material [1]. In recent years F and Cl have been measured in suites of melt inclusions from Iceland using both EPMA and SIMS [e.g., 2, 3] however no Br or I concentrations have been reported. The aim of our study was to determine the Br and I in suites of olivine- and plagioclase-hosted melt inclusions from Iceland. The melt inclusions were sampled from three sites in Iceland (Miðfell, Snæfellsjökull, and Oræfajökull). These melt inclusions have previously been analysed for major elements (EPMA), trace elements (SIMS), REE (SIMS) and F and Cl (SIMS).

Prior work

Halogen bearing basaltic glass standards were generated to assist developing an analytical setup. The basaltic glasses containing the melt inclusion hosting crystals were used as a starting material and doped with salts to create a specified halogen concentration. Standards of both tholeiitic and alkalic compositions were produced. The compositions of major elements and halogens in the glass standards were measured by EPMA to determine if the doping procedure was successful. We detected the presence of F, Cl and Br. Iodine measurements were very close to or lower than the detection limit (~90 ppm). It may be that iodine was lost in the production of the glasses, as we expected concentrations above 100 ppm. Further work was planned to measure the halogens by LA-ICP-MS to independently measure their halogen concentrations however this work has been inevitably delayed due to the COVID-19 pandemic.

Results and Analytical Challenges

Initial work involved determining the Br and iodine concentration in the doped glass standards at a mass resolution of 22,000. Br and iodine were standardised relative to GSE. Initial results show that we have successfully produced Br glass standards, two of alkalic composition with ~1000ppm and ~100ppm Br and iodine and one of tholeiitic composition ~1500ppm Br and iodine.

Br analysis in the melt inclusions was challenging, partially due to doming in the epoxy mounts.

The mounts have been re-polished to provide a flat surface and a standard added (GSE). Initial analysis of melt inclusions indicate very low concentrations of Br (<1-2ppm), but $^{79}Br/^{81}Br$ ratio scattering away from a ratio of ~1 (Fig. 1) suggests the presence of an interference on the shoulder on the ^{79}Br peak.

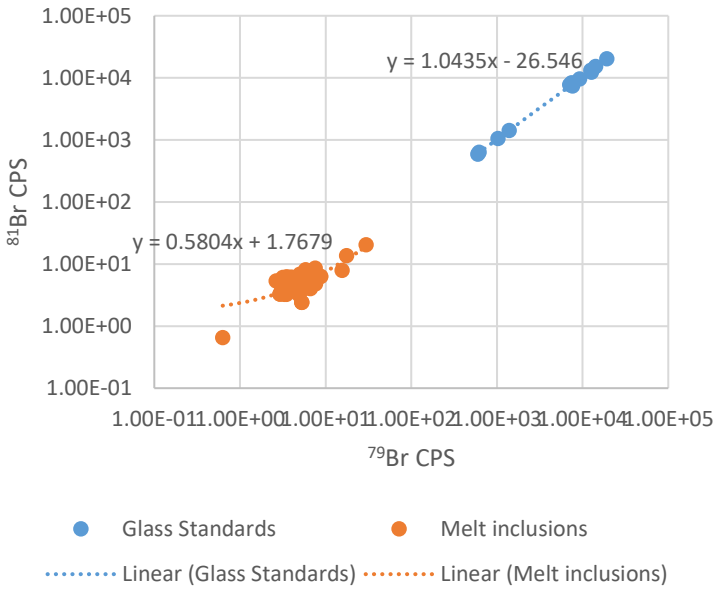

Fig. 1. Bromine ion ratios for glass standards and melt inclusions

Further issues were encountered in measuring iodine, which is expected to be <90 ppm from initial EPMA work. The gold coat used on the samples was found to contain trace quantities of iodine (Fig. 2), likely originating from the use of iodine in the gold extraction process. The iodine contamination of the gold coat and expected low abundance of iodine in the standards mean the concentrations measured by SIMS (10-40 ppm) may be have a large contribution from the gold coat. Measurements from the melt inclusions were <1 ppm and again are possibly influenced by the presence of iodine in the gold. Further without the completion of LA-ICP-MS we do not have an independent confirmation on the iodine concentration of the glass standards.

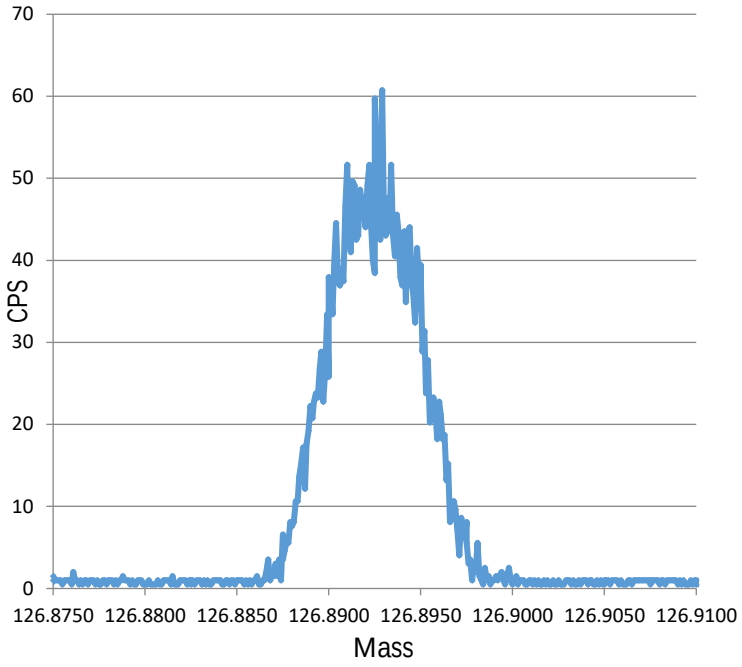

Fig. 2. Ion peak detected from gold coat

Future Work

The sample blocks have been prepared with a flatter surface and standards embedded in each sample block. Another attempt will be made to measure both Br and iodine in the melt inclusions with improvements to the epoxy blocks, however success is reliant on Br concentrations >3 ppm and an iodine-free gold coat being found. The doped glass standards have had some success and we are looking to further develop the work on these standards and calibrations for Br and I analysis.

References

[1] M. Kendrick et al. (2012) Geology, 44, 679-682
[2] M. E. Hartley et al. (2018) Contributions to Mineralogy and Petrology 173, 10
[3] D. A. Neave et al. (2014) Earth and Planetary Science Letters 400, 272-283

Appendix: analytical setup.

Analytical setup parameters are detailed on the next two pages.

Edinburgh Ion MicroProbeFacility

CAMECA: Cameca ims 1270 Date: 10/20/20
FILE NAME: C:\jcion5\Input\EW-GSE@6.asc

ACQUISITION PARAMETERS:

Species	Mass	B Field	Offset	C Time	W Time	Detector
76	76.000000	2019099	0.0	60.00	6.00	EM
30Si O3	77.958515	2043377	0.0	2.00	2.50	EM
79Br	78.918336	2056048	0.0	5.00	1.50	EM
81Br	80.916289	2082095	0.0	5.00	2.50	EM
126	126.000000	2602275	0.0	40.00	6.00	EM
127I	126.904473	2611787	0.0	5.00	1.00	EM

ANALYTICAL PARAMETERS:

Sample HV (v)	-9995
Field App. (um)	1506
Entr. Slit (um)	20
Exit Slit (um)	60
Energy Slit (eV)	61
Raster Size (um)	0
Cont. Aperture (um)	400
MRP (mono)	22289
Pressure (mb)	1.4E-8
PRIMARY Ion Species	Cs+
Primary HV (kV)	-3.90
Duo. Pressure (mbar)	6.1E-8
L4 Aperture (um)	200
Primary Beam (A)	4.232943E-9

ACQUISITION CONTROL PARAMETERS:

Pre-sputtering	SELECTED
Reference Signal	NOT SELECTED
Mass Calibration Control	SELECTED
Energy Control	NOT SELECTED
Beam Centering	SELECTED
EM HV ADJUST	N/A

DETECTOR PARAMETERS

Detector	Yield	Back Ground	Deadtime
FC1	1.000000	1386369	0.0

EM	0.987600	0	51.0
FC2	1.000000	-86463	0.0

Pre-Sputter Parameters

Selected	Duration (Seconds)	Raster Size Start (um)	Raster Size End (um)	Beam Selection Start	Bean Selection End
True	30	0	0	1 um	1 um

BEAM CENTERING:

Selected	Field Aperture	Entrance Slits	Contrast Aperture	Option1	Option2
True	yes	no	no		

Petrological insights into the volatile budget of the 2018 Kīlauean eruption

P.E. Wieser[1], H. Lamadrid[2], M. Edmonds[1], J. Maclennan[1], F.E. Jenner[3], C. Gansecki[4], R.L Lee[5], F. Trusdell[5], S. Matthews[6] & K. Iacovino[7]

[1]Department of Earth Sciences, University of Cambridge, UK
[2]Geological Sciences, University of Missouri, 65211, US
[3]School of Environment, Earth and Ecosystem Sciences, The Open University, MK7 6AA, UK
[4]University of Hawai'i, Hilo, [5]Hawaii Volcano Observatory, [6]John Hopkins University, [7]Jabobs, NASA

Background and Rationale

The 2018 eruption marked the most significant change in eruptive character at Kīlauea Volcano in the last 35 years, terminating the long-lived Pu'u 'Ō'ō eruption. Twenty four separate fissures opened in the Lower East Rift Zone between the 3rd and 27th of May, with activity localizing at Fissure 8 (F8) by the end of May [1]. The early fissures tapped relatively evolved, rift-stored magmas. Throughout May, glass and crystal compositions became increasingly primitive, as summit-derived magma flushed out the rift-zone storage reservoirs. These progressive changes in chemistry were interrupted by relatively explosive outbursts of highly evolved andesitic lava from F17 [2]. Constraining the volatile budget of this eruption is vital for two reasons. Firstly, it is currently uncertain exactly which reservoir beneath Kīlauea's summit supplied the magma erupted in 2018. Secondly, the lava erupted from the early fissures are among the most differentiated samples ever collected at Kīlauea, providing novel constraints on the evolution of volatiles during fractional crystallization at ocean island volcanoes.

Results and Discussion

We performed in-situ analyses of ~350 olivine-, pyroxene- and plagioclase-hosted melt inclusions and co-erupted matrix glasses by SIMS (H_2O, CO_2, F), Raman spectroscopy (vapour bubble CO_2), EPMA (major elements, Cl, S), and LA-ICP-MS (~60 lithophile and chalcophile elements). Our samples incorporate differentiated rift-stored basalts from early May (MgO_{glass}=3.6–4.9 wt%), a time series of the activity at F8 (May 7th to August 1st, MgO_{glass}=5.9–6.7 wt%), as well as the extremely differentiated compositions erupted at F17. In contrast to whole-rock data[2], our glass measurements classify this composition as dacitic (MgO_{glass}=1 wt%, $SiO_{2\ glass}$=65 wt%, Na_2O+K_2O=6 wt%).

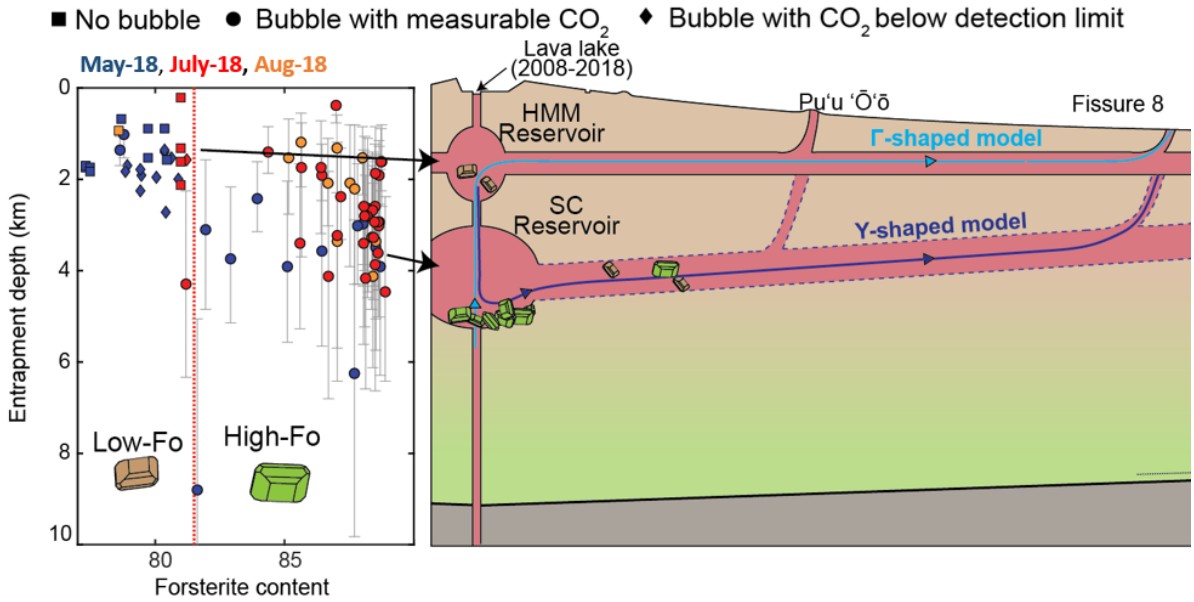

Fig. 1. Schematic diagram of magma storage feeding Fissure 8 between late May and August informed by melt inclusion saturation pressures.

The forsterite contents of olivine crystals erupted at Fissure 8 between Late May and August, together with the degree of major element disequilibrium with carrier melts, indicates that two distinct crystal populations were erupted (termed high and low-Fo). Melt inclusion entrapment pressures reveal that low-Fo olivines (close to equilibrium with their carrier melts) crystallized within the Halema'uma'u reservoir (~2-km depth; Fig. 1), while many high-Fo olivines (>$Fo_{81.5}$; far from equilibrium with their carrier melts) crystallized within the South Caldera reservoir (~3–5-km depth; Fig. 1). Melt inclusions in high-Fo olivines experienced extensive post-entrapment crystallization following their incorporation into cooler, more evolved melts. This favored the growth of a CO2-rich vapor bubble, containing up to 99% of the total melt inclusion CO2 budget (median = 93%). If only the glass phase had been measured by SIMS, magma storage depths would have been underestimated by a factor of ~10x. Conversely, reconstructions using equation of state methods rather than direct measurements of vapor bubbles overestimate entrapment depths. Overall, we show that measurements of melts and vapor bubbles by secondary-ion mass spectrometry and Raman spectroscopy, combined with use of a suitably calibrated H_2O-CO_2 solubility model, is a powerful tool to identify the magma storage reservoirs supplying volcanic eruptions.

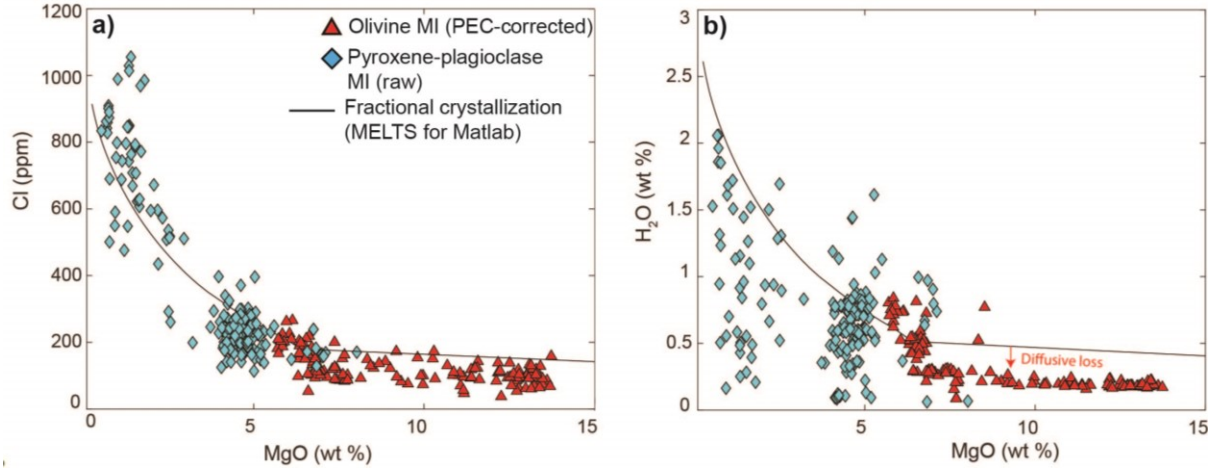

Fig. 2. Melt inclusion Cl and H_2O contents behave incompatibly during extensive fractional crystallization from basaltic andesite-dacitic compositions.

The more evolved melts erupted in the first two weeks of the eruption are variably enriched in incompatible trace and volatile elements such as Zr, Cl, and F (4-5x enrichment between 6-0.5 wt% MgO; Fig. 2). Melt inclusion data reveals that although the magmas are saturated in a mixed fluid throughout the fractionation interval, the high proportion of CO_2 in the co-existing fluid meant that melt H_2O contents followed a similar trajectory to incompatible elements such as Zr, with the most evolved dacitic melt inclusions having ~2 wt% H_2O. Coupled with a ~50-fold increase in magma viscosity, this H_2O-enrichment accounts for the explosive, Strombolian eruption style exhibited by dacitic melts erupted at Fissure 17 compared to the low fountaining/spattering observed at fissures erupting basaltic to basaltic-andesite compositions. Melt inclusion and matrix glass Nb/Y ratios of the evolved melts are most similar to those erupted from the 1955 eruption in the same region of the rift zone, indicating that the variably-evolved melts erupted in 2018 were generated by the crystallization of melts remaining in the rift zone after this eruption. Melt inclusion saturation pressures indicate that this parent magma body (or bodies) was stored at ~0.4-0.7 kbar (~2 km depth), which is in remarkable agreement with the depth at which a dacitic magma was intercepted during drilling in 2005 (~2488 m); and with a seismically-imaged Vp/Vs anomaly. Highly evolved, volatile-rich melts with potential for hazardous, explosive eruptions may be lurking at depth within many OIB systems, with dyke injection (or hydrothermal drilling) providing a pathway by which these melts can ascend to the surface.

References

[1] https://volcanoes.usgs.gov/vsc/file_mngr/file-179/Chronology%20of%20events%202018.pdf. [2] Gansecki et al., (2019). Science 366, 10.1126/science.aaz1822.